

OLD DOMINION UNIVERSITY RESEARCH FOUNDATION

DEPARTMENT OF MECHANICAL ENGINEERING AND MECHANICS
SCHOOL OF ENGINEERING
OLD DOMINION UNIVERSITY
NORFOLK, VIRGINIA

(NASA-CR-153935) RESULTS OF
GRAPHITE-POLYIMIDE ISOGRID PANEL TESTING N77-28229
Interim Report (Old Dominion Univ. Research
Foundation) 57 p HC A04/MF A01 CSCL 11D Unclas
G3/24 39197

RESULTS OF GRAPHITE-POLYIMIDE ISOGRID PANEL TESTING

By

M.W. Hyer

and

Dale O. Douglas

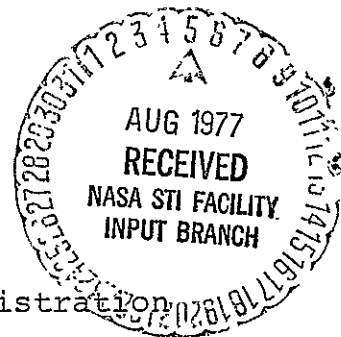
Interim Report

Prepared for the
National Aeronautics and Space Administration
Langley Research Center
Hampton, Virginia 23665

Under
Research Grant NSG 1167
Dr. John G. Davis, Jr., Technical Monitor
Materials Division

Submitted by the
Old Dominion University Research Foundation
Norfolk, Virginia 23508

June 1977



Old Dominion University Research Foundation



Norfolk, Virginia 23508

Phone 804/489-6624

August 1, 1977

Dr. John G. Davis, Jr.
National Aeronautics and Space Administration
Langley Research Center - Mail Code 188A
Hampton, VA 23665

Dear Dr. Davis:

Reference research grant NSG 1167, Michael W. Hyer principal investigator.

Enclosed is an interim report on work performed under the referenced grant.

Please contact this office if you have any questions on the report.

Sincerely,

A handwritten signature in cursive script that reads "Maxine Lippman".

Maxine Lippman
Publications Coordinator (Acting)

Encl: Int Rpt, 3 cys

cc: NASA Sci & Tech Info Fac, 2 cys
Dr. Hyer, 12 cys
Dr. Goglia, 1 cy
ODU Library, 1 cy
Mr. Kawalkiewicz, 1tr only

/mal

DEPARTMENT OF MECHANICAL ENGINEERING AND MECHANICS
SCHOOL OF ENGINEERING
OLD DOMINION UNIVERSITY
NORFOLK, VIRGINIA

RESULTS OF GRAPHITE-POLYIMIDE ISOGRID PANEL TESTING

By

M.W. Hyer

and

Dale O. Douglas

Interim Report

Prepared for the
National Aeronautics and Space Administration
Langley Research Center
Hampton, Virginia 23665

Under
Research Grant NSG 1167
Dr. John G. Davis, Jr., Technical Monitor
Materials Division



June 1977

TABLE OF CONTENTS

	Page
1.0 INTRODUCTION	1
2.0 DESCRIPTION OF THE PANELS	1
3.0 ANALYSIS	2
4.0 PANEL TESTING	6
4.1 Testing of Isogrid Panel 7	6
4.2 Testing of Isogrid Panel 8	10
4.3 Testing of Isogrid Panel 9	13
5.0 CONCLUSIONS	15
REFERENCES	52

LIST OF FIGURES

Figure 1. Isogrid panel 7.	17
Figure 2. Isogrid panel 8.	18
Figure 3. Imperfections in panel 7, back side.	19
Figure 4. Imperfections in panel 8, front side.	20
Figure 5. Imperfections in panel 8, back side.	21
Figure 6. Panel geometry.	22
Figure 7. Skin-stiffened panel 9, back view.	23
Figure 8. Skin-stiffened panel 9, front view.	24
Figure 9. Top and bottom end fittings.	25

LIST OF FIGURES--continued

	Page
Figure 10. Knife edges for longitudinal side support.	26
Figure 11. Strain gage and DCDT location, panel 7.	27
Figure 12. In-plane load-deflection behavior, panel 7.	28
Figure 13. Out-of-plane deflection of node 6, panel 7.	29
Figure 14. Out-of-plane nodal deflections, panel 7, load = 1808 N.	30
Figure 15. Out-of-plane nodal deflections, panel 7, load = 6142 N.	31
Figure 16. Out-of-plane nodal deflections, panel 7, load = 12751 N.	32
Figure 17. Effect of initial imperfection on force versus moment for a beam-column.	33
Figure 18. Force versus moment across gaged section of panel 7.	34
Figure 19. Strain versus force for gages 1, 16, 33, and 48 on panel 7.	35
Figure 20. Modified end fittings for panel 8.	36
Figure 21. Strain gage and DCDT location, panel 8.	37
Figure 22. Panel 8 in test fixture.	38
Figure 23. In-plane load-deflection behavior of panel 8.	39
Figure 24. Out-of-plane nodal deflections, panel 8, load = 1860 N.	40
Figure 25. Out-of-plane nodal deflections, panel 8, load = 6212 N.	41
Figure 26. Out-of-plane nodal deflections, panel 8, load = 13065 N.	42
Figure 27. Out-of-plane nodal deflections, panel 8, load = 18766 N.	43

LIST OF FIGURES--concluded

Page

Figure 28.	Strain versus load for back-to-back gage pairs 19-20, 21-22, and 23-24.	44
Figure 29.	Strain versus load for back-to-back gage pairs 1-2 and 17-18.	45
Figure 30.	Strain gage and DCDT locations, panel 9.	46
Figure 31.	Separation of skin and framework on skin-stiffened panel.	47
Figure 32.	Moiré fringe pattern on panel 9 at no-load condition.	48
Figure 33.	Moiré fringe pattern on panel 9 at intermediate load level.	49
Figure 34.	Moiré fringe pattern on panel 9 at panel failure.	50
Figure 35.	In-plane load-deflection behavior for panel 9.	51

RESULTS OF GRAPHITE-POLYIMIDE ISOGRID PANEL TESTING

By

M.W. Hyer¹ and Dale O. Douglas²

1.0 INTRODUCTION

Polyimide resins offer the potential of using fiber-reinforced composites in structures required to operate at elevated temperatures. McDonnell-Douglas, under contract with-NASA Langley Research Center, conducted a program to develop a procedure for fabricating short-fiber HTS graphite and NR150B2 polyimide resin into an isogrid configuration. The program involved molding tool development, molding cycle development, testing samples for material properties, and fabricating several panels. Two of the panels were open isogrid panels while a third panel was reinforced with a T300/NR150B2 polyimide skin. After fabrication, the panels were given to the Langley Research Center for structural analysis and testing. The testing program is the subject of this report. Details of the fabrication are given in reference 1.

2.0 DESCRIPTION OF THE PANELS

Figures 1 and 2 show open isogrid panels 7 and 8, respectively. The two open isogrid panels are identical except for minor imperfections. These are circled in the figures. Initially, McDonnell-Douglas had problems with resin starving

¹ Assistant Professor, Department of Mechanical Engineering and Mechanics, Old Dominion University, Norfolk, Virginia 23508.

² Research Assistant, Department of Mechanical Engineering and Mechanics, Old Dominion University, Norfolk, Virginia 23508.

during the fabrication process and six panels were fabricated before a satisfactory panel resulted. However, no panel was completely free of resin starving but on the test panels there were only a few isolated areas.

The imperfections in panel 7 did not penetrate the legs in the grid work as deeply as the imperfections in panel 8 and were most obvious from the back. Figure 3 shows a detail of the back of panel 7 in the area of the imperfections. Figures 4 and 5 show details of the front and back sides, respectively, of panel 8 in the area of the imperfections.

Figure 6 shows the geometry of the panel. In order to enhance the release of the panel from the mold, there was a slight taper in the width of the members in the thickness direction.

Figures 7 and 8 show the isogrid panel with skin. The skin was 1.016 mm thick and was bonded to the grid work with American Cyanamide's FM34 adhesive.

3.0 ANALYSIS

The panels were to be loaded in compression with a uniform in-plane loading across the top and bottom end of the panel and supported on all four sides. An equivalent plate theory was developed by McDonnell-Douglas to predict the in-plane load-deflection behavior, buckling load and proportion of load carried by the central lattice and longitudinal side edges. The equivalent plate method of analysis was done by determining "smeared out" stiffnesses and thicknesses so the panels could be considered as a solid, continuous sheet of material with appropriate geometric and elastic properties. Classical plate equations (see for example ref. 2) could then be used to predict the behavior.

The procedure for determining the equivalent continuous panel is based on first principles from theory of elasticity and

Kirchhoff plate theory. The procedure is quite straightforward, but it is not necessary to go through this procedure for each panel because, as a result of the analysis, simple relations exist between the parameters of the isogrid panel, such as triangle height, rib width, rib thickness, Young's Modulus, etc., and the parameters for an equivalent, solid, continuous plate. The formulas are repeated here for convenience. The number in parenthesis after the various formulas are the values used here in comparisons between experiment and theory.

The equivalent Young's Modulus, E^* , for an open isogrid panel is given by

$$E^* = E \frac{b}{h} \quad (1)$$

where

E = Young's Modulus of the material (105×10^9 N/m²)

b = rib width (3.33 mm)

h = height of one isogrid triangle (41 mm)

For the skin stiffened panel E^* is given by

$$E^* = E \frac{(1 + \alpha)^2}{\beta} \quad (2)$$

$$\alpha = \frac{bd}{th} (.304)$$

t = skin thickness (1.016 mm)

d = rib thickness (3.81 mm)

$$\beta = [3\alpha(1 + \delta)^2 + (1 + \alpha)(1 + \alpha\delta^2)]^{1/2} \quad (5.24)$$

$$\delta = \frac{d}{t} \quad (3.75)$$

and the equivalent panel thickness, t^* , is given by

$$t^* = t \frac{\beta}{1 + \alpha} \quad (3)$$

These equivalent values can be substituted into the equation for critical buckling load, assumed by McDonnell-Douglas to be

$$N_{cr} = \frac{3.29}{1 - \nu^2} \frac{Et^3}{w^3} \quad (4)$$

where

N_{cr} = buckling load

E = Young's Modulus

t = panel thickness

w = loaded width

ν = Poisson's ratio = .3 (ref. 1, p. 30)

Equation (4) assumes a square plate simply supported on four sides. This formula is conservative in that a rectangular plate, which is the case of the isogrid panels, can support higher loads, depending on aspect ratio. Using the outside dimensions, the aspect ratio for the isogrid panels is 1.39. Using this, the equation for the critical buckling load is

$$N_{CR} = \frac{4}{1 - \nu^2} \frac{Et^3}{w^3} \quad (5)$$

The proportion of the in-plane load carried by the grid and longitudinal sides was determined by assuming the applied load causes an in-plane deflection which is uniform across the ends and by assuming the grid acts as a whole and each side individually, resulting in three components resisting in-plane compression. With the in-plane deflection being uniform across the ends, each component is subject to the same strain and with the in-plane E of the grid, the E of the side pieces and the respective areas, the load in each component can be determined. The results are

$$\frac{P_2}{P_1} = \frac{2\ell_1 h}{b\ell_2} \quad (6)$$

where

$$\frac{P_1}{2} = \text{load carried by one longitudinal side}$$

$$P_2 = \text{load carried by grid}$$

$$P_1 + P_2 = \text{total load carried by panel}$$

$$\ell_1 = \text{width of side piece (6.6 mm)}$$

$$\ell_2 = \text{width of grid area (170.7 mm)}$$

$$h = \text{height of one isogrid triangle (41 mm)}$$

$$b = \text{rib width (3.33 mm)}$$

Note, the proportioning of load is independent of E . Underlying this is the assumption that E doesn't vary from position to position on the panel. As noted previously, the value of E actually used in the calculations was taken to be $105 \times 10^9 \text{ N/m}^2$, a value provided by McDonnell-Douglas (ref. 1, p. i).

4.0 PANEL TESTING

4.1 Testing of Isogrid Panel 7

Open isogrid panel number 7 was tested with the testing fixture supplied by McDonnell-Douglas. The fixtures were designed to simulate simple supports on all four sides. The top and bottom ends of the panel were potted in fittings shown in figure 9 using HYSOL TC-5467/HD-0111. The fittings were partially sawed through so that when the panel started to buckle the material in the cut region would yield, forming a plastic hinge which would produce little resistance to rotation but would restrict out-of-plane displacement. The longitudinal edges of the panel were restricted from out-of-plane displacement by the knife edges shown in figure 10. The slots in the knife edge supports allowed the knife edges to be clamped tightly enough along the longitudinal edges so the knife edges did not need additional support. However, as a precaution, the bottom end of the knife edges were resting on compressible rubber pads. Since the upper and lower ends of the panel could not displace out-of-plane and the knife edges did not allow curvature to develop, the displacement of the panel was zero along the longitudinal edges. However, due to expected in-plane shortening of the panel, due to the compressive in-plane load, the knife edges were shorter than the distances between the end fittings. When mounted in the test fixture, there was about .20 mm length of unsupported longitudinal edge at the top end of the knife edge.

The panel response was measured with strain gages and direct-current displacement transducers (DCDT). Figure 11 shows the

locations of the measurements. Strain gages 1, 16, 33, and 48 measured the uniformity and magnitude of the loading through the longitudinal sides, and gages 25 through 32 and 34 through 47 measured the load supported by the grid. Due to the small size of the panel and the lack of symmetry, it was felt that perhaps a representative leg did not exist so all legs were gaged. The out-of-plane displacement of each node was measured with a DCDT. In addition, the in-plane shortening of the panel was measured with a DCDT. The panel was mounted in the loading machine so the observer would normally view the panel with an orientation shown in figure 11 and with the narrower widths of the mold-release tapered legs closest to the observer. Note that in figures 1 to 5, the orientations of the panels vary from the orientation shown in figures 6 and 11. All subsequent discussions refer to the orientation in figure 11.

After several low level loadings to check instrumentation and to check for any unexpected eccentricities, the panel was loaded to failure. As the load was increased from zero the panel began to bow. In general, the out-of-plane deflections varied linearly with load up to about 6200 N and reached 0.1 mm at the center of the panel. After that level, the out-of-plane deflections began to increase more rapidly with load. Initially, the bottom row of nodes moved out-of-plane in a direction opposite to the movement of the other rows. As the load increased, the bottom row reversed direction, and all nodes moved in the same direction (away from the observer when referring to fig. 11). Figure 12 shows the in-plane load-deflection behavior and figure 13 shows the out-of-plane deflection at node 6, a representative node. After 8800 N the exact sequence of events is uncertain; however, at about 8800 N, a plastic hinge formed at the partial cut in the top end piece and the piece began to rotate. Referring to figure 13, it is evident that the out-of-plane deflections, and thus the rotation of the plastic hinge, continued to increase substantially. The rotation of the hinge was limited by the width of the saw cut, a gap of .508 mm. However, accompanying the rotation of the end piece was a bending failure of the longitudinal edge pieces above the knife edges, in the gap left

for in-plane shortening. The failure above the knife edge was unexpected, but as soon as the plastic hinge formed and allowed rotation, the only place the longitudinal edge pieces could develop curvature was in the region not supported by the knife edge. The leveling off in load at the end of the in-plane load-deflection history, figure 12, is attributable to this bending failure.

It is impossible to determine what the load capacity of the panel would have been had the longitudinal sides not failed in bending. However, in-plane stiffnesses (in-plane E) and proportion of total load through the ribs and longitudinal sides could be calculated.

Using the slope of the in-plane load-deflection curve (fig. 12), in-plane Young's Modulus is determined to be

$$E_{\text{in-plane}} = 7.2 \times 10^9 \text{ N/m}^2$$

Using equation (1), the theoretically predicted value of the in-plane Young's Modulus is

$$E_{\text{in-plane}} = 8.45 \times 10^9 \text{ N/m}^2$$

The proportioning of the total load was determined using strain data from the gaged ribs and longitudinal side pieces. For a total load of 1808 N,

$$\frac{P_2}{P_1} = .72$$

For a total load of 6142 N

$$\frac{P_2}{P_1} = .70$$

This compares with $\frac{P_2}{P_1} = .95$ from equation (6) which, of course, is load-independent.

Figures 14, 15, and 16 show, respectively, the nodal deflections at three load levels: a low load, 1808 N, and two higher loads, 6142 N and 12751 N. Generally, small imperfections would determine the deflection behavior at low load levels while the buckling mode shape would determine the deflections at higher loads. On the other hand, large imperfections would dominate the deflections at all load levels. Thus a comparison of out-of-plane displacements at high and low load levels would indicate the degree to which imperfections dominate the buckling behavior. However, since bending of the longitudinal sides above the knife edges dominated the deflections at high load levels, it is not certain that the comparison is meaningful in this case. Since, as seen in figures 14, 15, and 16, the lower row of nodes moved in a direction opposite of the other nodes and node 15 remained stationary, as the load was increased, local imperfections somewhat governed the behavior. At the high load level, the top end out-of-plane deflections would necessarily be larger because the bending of the longitudinal sides at that end deflected the top backwards. During the loading process, local failures were observed at some of the nodes causing discontinuities in slope and no doubt contributing to the behavior of neighboring nodes.

As a matter of interest, another measure of imperfection was calculated. It is based on the following argument. Referring to figure 17, a column with an initial eccentricity of e and a deflection d , measured from the unloaded position, induced by load F will have an internal moment, M , given by

$$M = F (e + d)$$

Writing this as

$$M = Fe \left(1 + \frac{d}{e}\right) = Fd \left(1 + \frac{e}{d}\right)$$

it is obvious for small $\frac{d}{e}$, i.e., when the load is small, the slope of the moment-force curve is $\frac{1}{e}$ while for small $\frac{e}{d}$, i.e., when the load is large, the slope is $\frac{1}{d}$. Figure 18 shows a plot of M across the gaged portion of the panel versus applied load. The moment was calculated using strains from the back-to-back gages on the grid legs. Since the longitudinal sides have no curvature at that point on the panel, they do not enter into the calculations for M . The plot indicates an initial eccentricity of 0.043 mm, not a large number considering the panel is 3.81 mm thick. However, this is an equivalent eccentricity and the result of effects which could, overall, cancel each other but locally have a strong effect. For example, the slight taper on the legs for mold release purposes shifts the neutral axis toward the rear of the panel. In addition, inspection of the panel before plotting indicated initial curvature in both directions. Based on the behavior of the nodes during loading, there were local effects which did not show up in this global eccentricity calculation.

Figure 19 indicates the strain in gages 1, 16, 33, and 48. It is evident that each leg carried approximately the same load and the load was uniform along its length.

4.2 Testing of Isogrid Panel 8

In order to avoid problems with the plastic hinge rotation and localized bending at the ends of the knife edges, the test fixtures were modified for the second open isogrid panel test. The simply supported end concept was replaced by fixed-end pieces. Longer knife edges, 262 mm in length, were fabricated and the end pieces designed so the knife edges could extend beyond the upper and lower ends of the panel but still allowing plane shortening of the panel. The modified end fittings are shown in figure 20.

Instead of having the potting channel extend across the entire width of the panel, the channel is shorter and cantilever extensions, approximately the same thickness as the panel, transmit the load to the longitudinal side pieces. This allows the knife edges to extend the entire length of the panel. The cantilever extensions are actually narrower than the panel thickness to insure that the knife edges contact the entire longitudinal side. The only concern was that the less stiff extensions might allow the longitudinal sides to unload slightly and transfer more load to the grid. The strain gage and DCDT layout was similar to the layout at the first isogrid panel and is shown in figure 21. Several of the legs in the gridwork were gaged for in-plane bending measurements. Back-to-back gages 19-20, 21-22, and 23-24 were for these measurements. Figure 22 shows panel number 8 in the test fixture, with one knife edge removed and without the DCDT's in position, and illustrates the arrangement with the end fittings and the longer knife edges. The knife edges are resting on rubber support pads.

Panel number 8 supported a considerably higher load than panel 7 but sustained a serious local out-of-plane buckling failure near node 72. Figure 23 shows the in-plane load-deflection characteristics and there is no evidence of this local failure, which occurred around 16500 N. However, the failure propagated rapidly to the surrounding nodes and rather than completely collapse the specimen, the test was terminated so the initial failure could be examined.

As the load was applied, the lower three rows of nodes moved backwards and continued in this direction as the load increased. However, the top row moved backward, then forward, with increasing load while the second row from the top reversed direction several times before finally moving forward. This behavior indicates that local imperfections influenced the behavior

of the displacements. At the higher load levels, the top two rows of nodes moved in a direction opposite the bottom three, indicating a tendency to buckle in a full sine-wave type shape. The nodal displacements at four load levels, 1860 N, 6212 N, 13065 N, and 18766 N are shown in figures 24, 25, 26, and 27, respectively. The local buckling, involving nodes 69 and 72, is evident in figure 27 by the larger out-of-plane deflection of these nodes.

Figure 28 shows the strains from the back-to-back gage pairs measuring the in-plane bending of selected legs. It is obvious there is very little in-plane bending in these three legs. Pairs 19-20 and 23-24 are well behaved while pair 21-22 is a bit erratic, presumably because it is near the edge of the grid where the load is being transferred from the longitudinal sides. Figure 29 shows back-to-back pairs on the longitudinal sides. The two sides appear to have been equally loaded, and there was a tendency, at least with the segments gaged, for the longitudinal sides to bend inward. The back-to-back pairs 3-4 through 15-16 indicated out-of-plane bending from no-load to the end of the test.

From figure 23, the in-plane Young's Modulus was computed to be

$$E_{\text{in-plane}} = 7.8 \times 10^9 \text{ N/m}^2$$

This figure is comparable with the number obtained from panel number 7.

The proportioning of total load through the gridwork and longitudinal sides was computed at several loads and is indicated as follows:

<u>In-plane Load</u>	$\frac{P_2}{P_1}$
1860 N	.72
6212 N	.74
13065 N	.74
18766 N	.59

Examination of the panel indicated the local failure near node 72 occurred in one of the legs that had a resin-starved imperfection. In figure 2 this is the imperfection in the upper right.

4.3 Testing of Isogrid Panel 9

The skin-stiffened isogrid panel was tested with the longer knife edges and the same type end fittings used for panel 8. The potting channels in the end fittings (see figure 20) were widened to accommodate the additional thickness of the skin. Rather than use a DCDT at each node, the shadow Moiré technique was used to determine behavior of the panel. The flat surface of the skinned side of the panel provided a good opportunity to use this method. Although Moiré can be used to obtain quantitative information regarding displacement, it was used here only to obtain qualitative information. The shadow Moiré technique measures the partial derivative of the out-of-plane displacement with respect to the direction perpendicular to the grid lines. Thus a fringe on a Moiré pattern represents the locus at points which have the same partial derivative. For the case at hand, the grid master lines were aligned vertically so the locus of points on a particular fringe represented points where the partial derivative of the out-of-plane displacement with respect to the horizontal direction was a constant.

Strain gages and DCDTs were used at selected points to further monitor the behavior of the panel. Figure 30 shows the strain

gage and DCDT locations. Rosettes 7-8-9, 16-17-18, and 25-26-27 were used to measure the shear strain in the skin at various locations. The other strain gages made up back-to-back pairs on various grid legs at several locations on the panel.

Basically the panel failed at a load of about 40050 N, due to separation of the skin from the isogrid backing over the lower 1/2 of the panel. This can be seen clearly in figure 31. In the failed configuration, the gridwork was bowed substantially backward while the skin was bowed forward slightly. The debonding appeared to start in the lower left hand corner at the panel (when viewed from the front).

Figures 32, 33, and 34 show the Moiré fringe patterns at 3 load levels. Figure 32 shows the fringe pattern with no load. Theoretically there should be no fringe pattern with no load but surface irregularities of the panel skin and lack of parallelism between the grid master plate and the panel result in initial fringe patterns. Apparent also in this photograph, to the right of the panel, is the DCDT used to measure in-plane shortening of the panels. The DCDT actually measures the change in distance between the lower and upper heads of the loading machine. This set-up was similar on all three panel tests. Figure 33 shows the fringe pattern at an intermediate load level. The dark, wide vertical line on the left of the panel is the shadow from the knife edge support. Recalling that the fringes measure displacement slopes across the panel, it is evident that the out-of-plane deflections are quite symmetric across the panel. However, there is a dissymmetry in the slopes from top to bottom, with the center of the concentric fringe pattern being closer to the bottom. At lower load levels the dissymmetry was more pronounced. Figure 34 shows the fringe pattern after debonding occurred.

The character of the displacement pattern from top to bottom was further illustrated by displacement measurements from the selected nodes. Nodes 67, 68, 69, 71, and 72 basically all moved backwards while 73 moved forward. This is indicative of either

local effects or the tendency to buckle into a full sine-wave type pattern. Although it is felt the skin would have a tendency to spread out local effects, this movement in opposite directions was confined to the top node and should be classified as a local effect.

The in-plane load-deflection behavior was not as well behaved as that of the other two panels. Referring to figure 35, the in-plane stiffness seemed to increase after a load of 8900 N and remained fairly constant until debonding occurred. Using the slope of the curve in figure 35 between 8900 N and 40050 N

$$E_{\text{in-plane}} = 17 \times 10^9 \text{ N/m}^2$$

The predicted value, using equation (2) is

$$E_{\text{in-plane}} = 34 \times 10^9 \text{ N/m}^2$$

The strain gage data showed there were reversals in curvature as the load was applied, but that in general the panel bowed backwards. The shear strain in rosettes 7-8-9 and 16-17-18 were approximately an order of magnitude less than the axial compressive strain in the rosette. Gage 25 malfunctioned so the shear strain could not be computed for rosette 25-26-27.

5.0 CONCLUSIONS

Local imperfections seemed to dominate the buckling behavior of the three isogrid panels. It may not be completely valid to draw this conclusion about the first panel since its failure was due to the support fixture. However, the node in the lower right-hand corner actually reversed directions while loading and thus represents some sort of local imperfection. The other two, however, failed due to local imperfections and in particular,

local material imperfections, the one being due to resin-starving and the other most likely due to adhesive failure.

As far as in-plane response is concerned, the open panels behaved pretty much as expected. The in-plane stiffness was less than predicted and the load carried by the grid, as opposed to the longitudinal sides, was less than expected for both open panels at all load levels. However, in-plane bending of the individual legs was not expected to be important and from the strain data, it apparently was not. The predicted in-plane stiffness for the skin-stiffened panel was high by a factor of two.

One possible explanation of the deviations between expectations and actual results is the size of the panel. It is reasonable to assume that the repetitive behavior of the gridwork did not begin until 1 or 2 nodes in from the longitudinal edges. The stiffening effects of the longitudinal edges penetrate the gridwork and for the individual triangles to act like an isotropic medium, there probably needs to be a certain number across the width. These panels had only 4 nodes across the width and thus perhaps the isogrid effect was never developed. In future work, larger panels could be constructed to overcome this problem. In addition, in future testing, it would be interesting to actually eliminate a leg (by cutting it out) to determine the effects of local imperfections or to determine how many legs can be removed before the panel is seriously affected.

ORIGINAL PAGE IS
OF POOR QUALITY

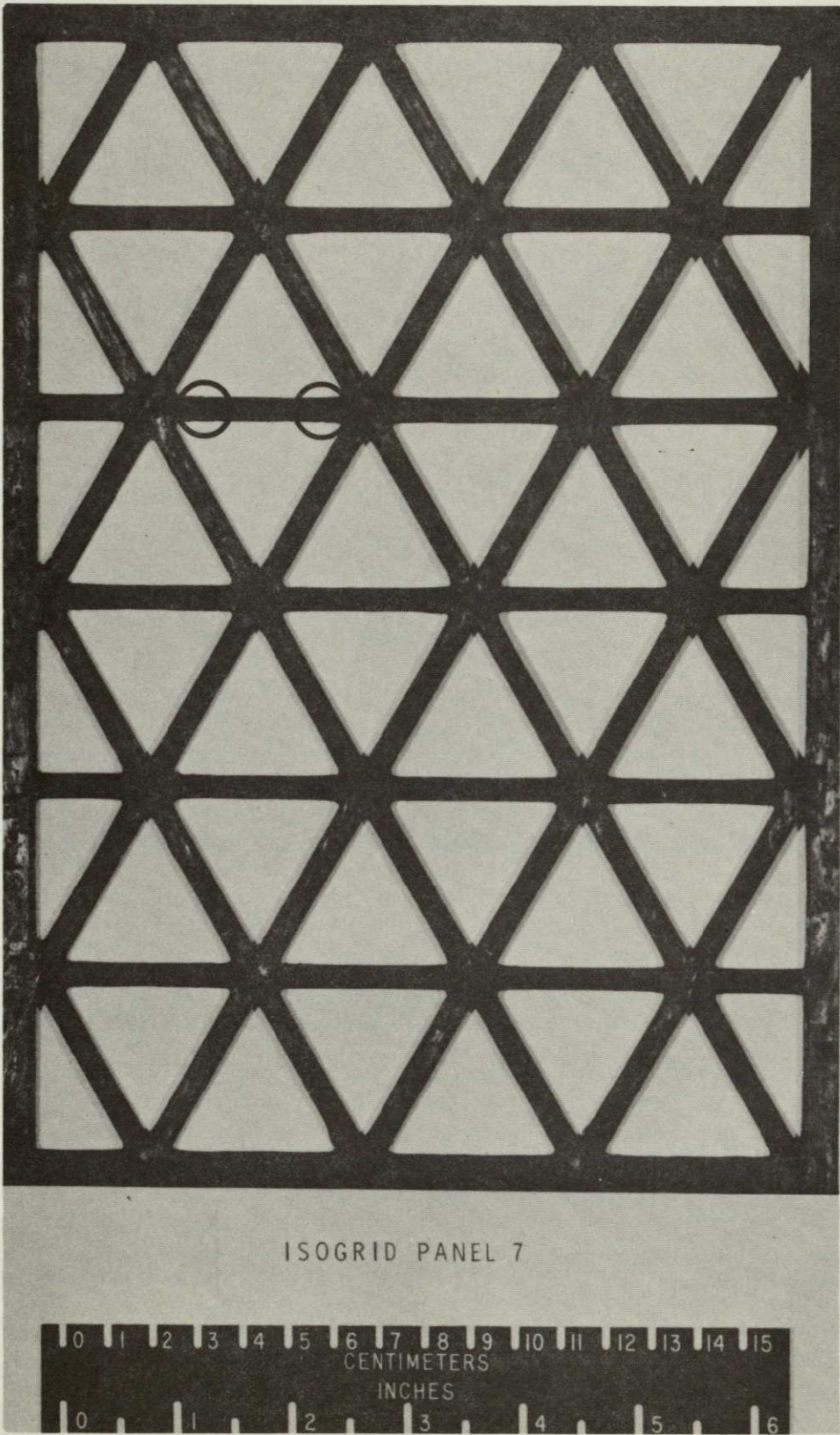
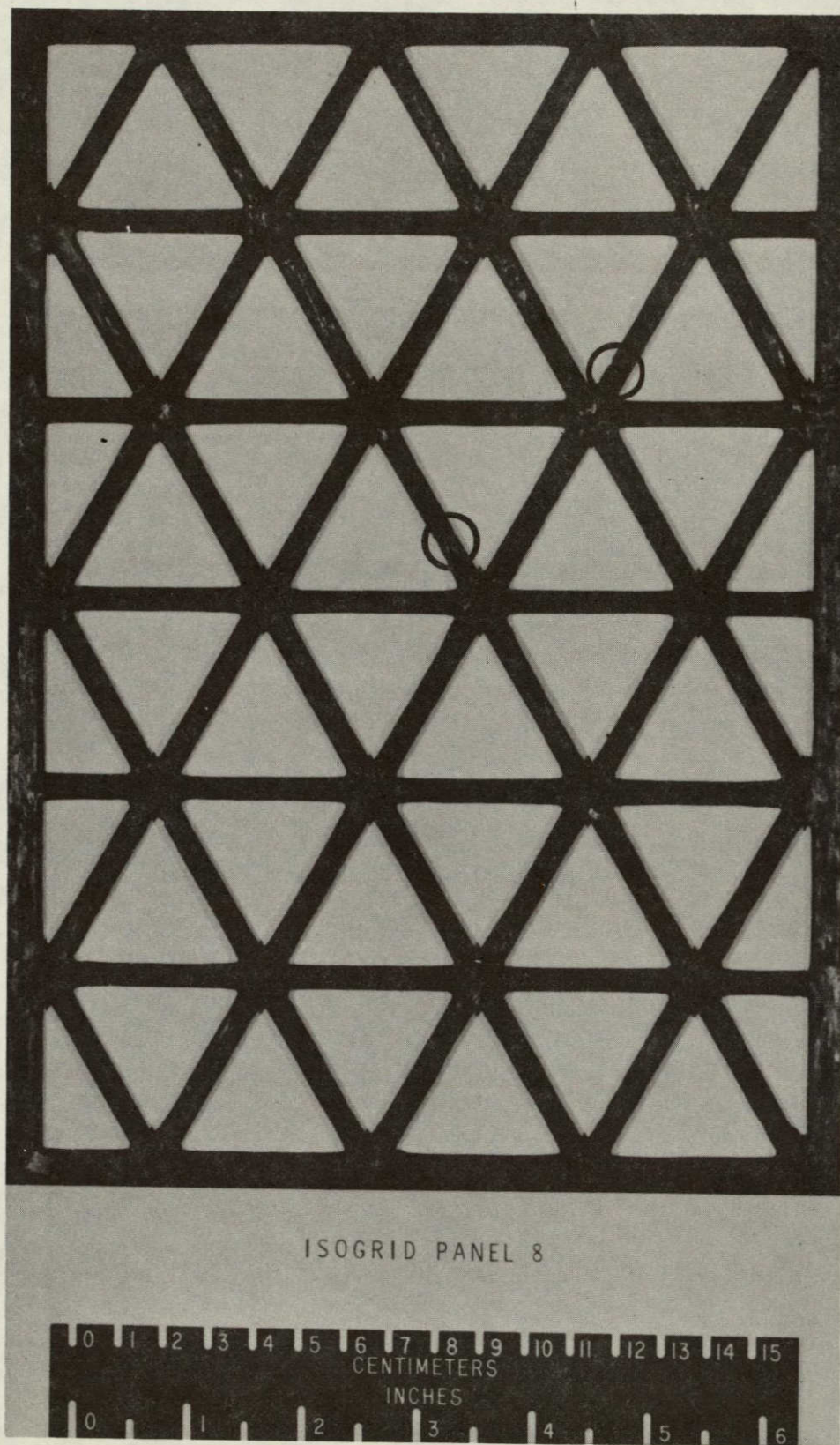


Figure 1. Isogrid panel 7.



ISOGRID PANEL 8

Figure 2. Isogrid panel 8.

ORIGINAL PAGE IS
OF POOR QUALITY

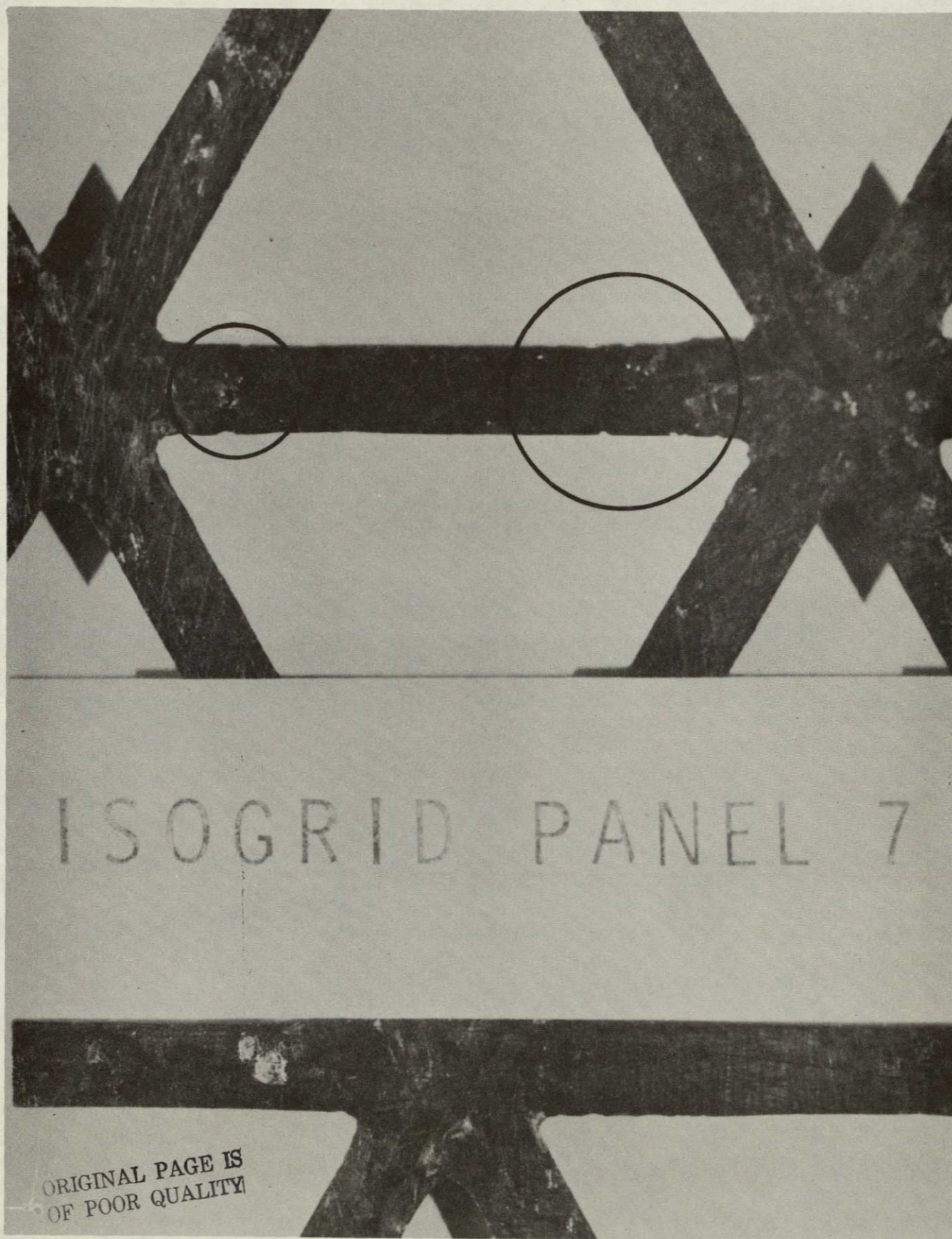
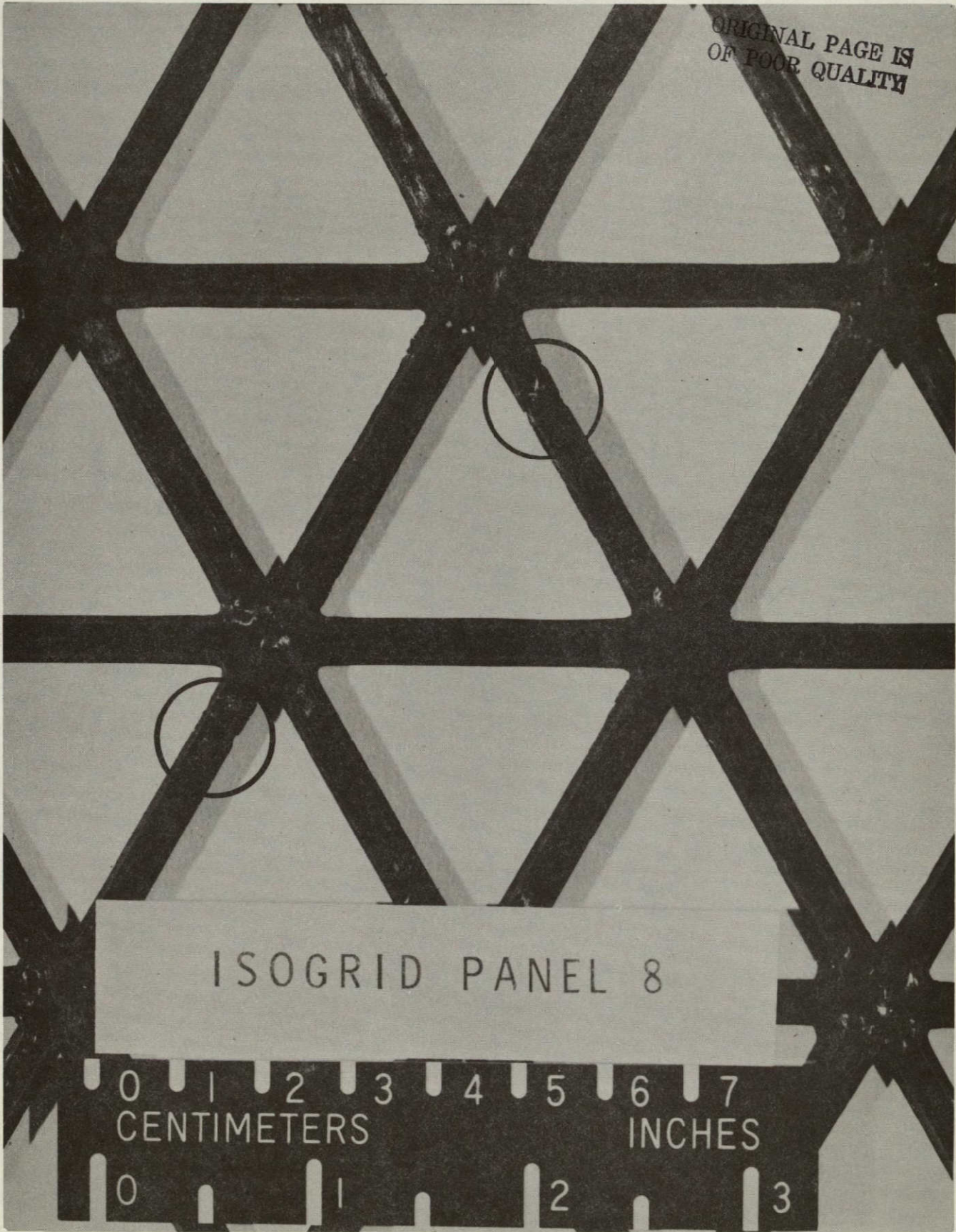


Figure 3. Imperfections in panel 7, back side.

ORIGINAL PAGE IS
OF POOR QUALITY




ISOGRID PANEL 8

0 1 2 3 4 5 6 7
CENTIMETERS INCHES

0 1 2 3

Figure 4. Imperfection in panel 8, front side.

ORIGINAL PAGE IS
OF POOR QUALITY

The image shows a repeating geometric pattern of dark, thick lines forming a grid of triangles. The lines intersect at various angles, creating a complex, interlocking structure. A small, dark, circular mark is circled in black on the left side of the pattern, indicating an imperfection. A white rectangular box is superimposed over the center of the image, containing the text 'ISOGRID PANEL 8'.

ISOGRID PANEL 8

Figure 5. Imperfection in panel 8, back side.

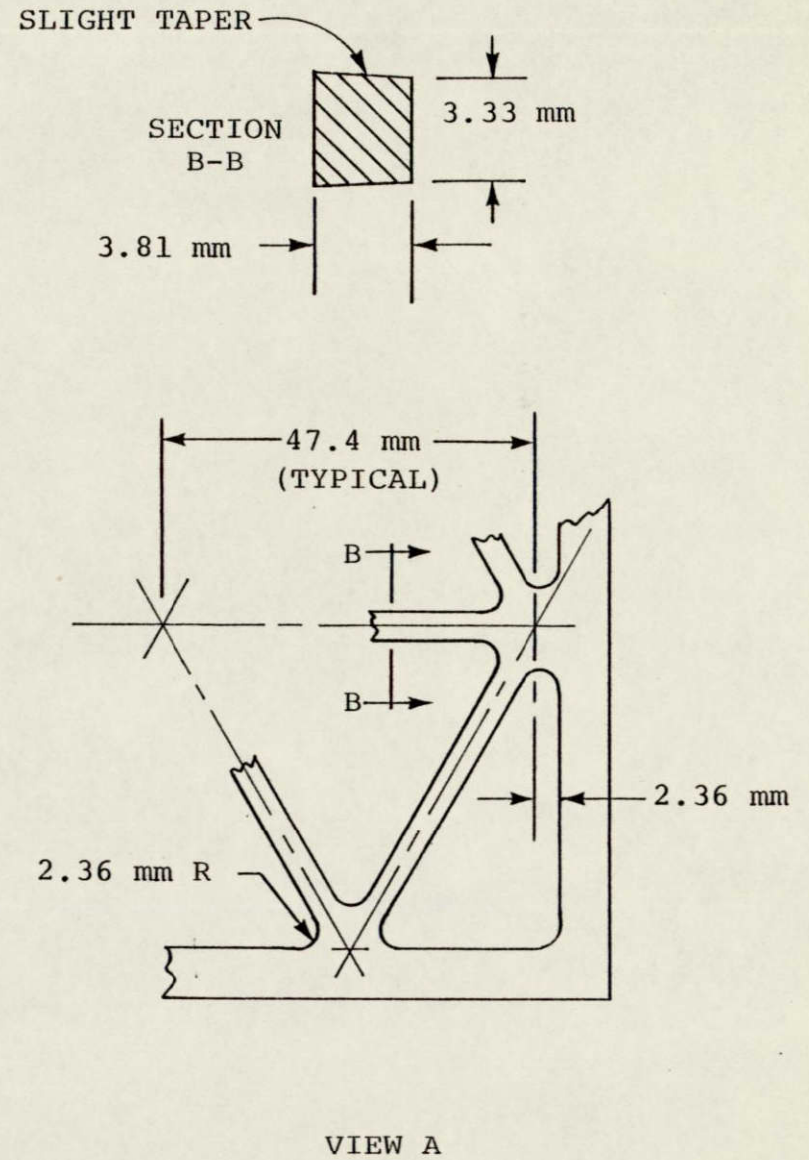
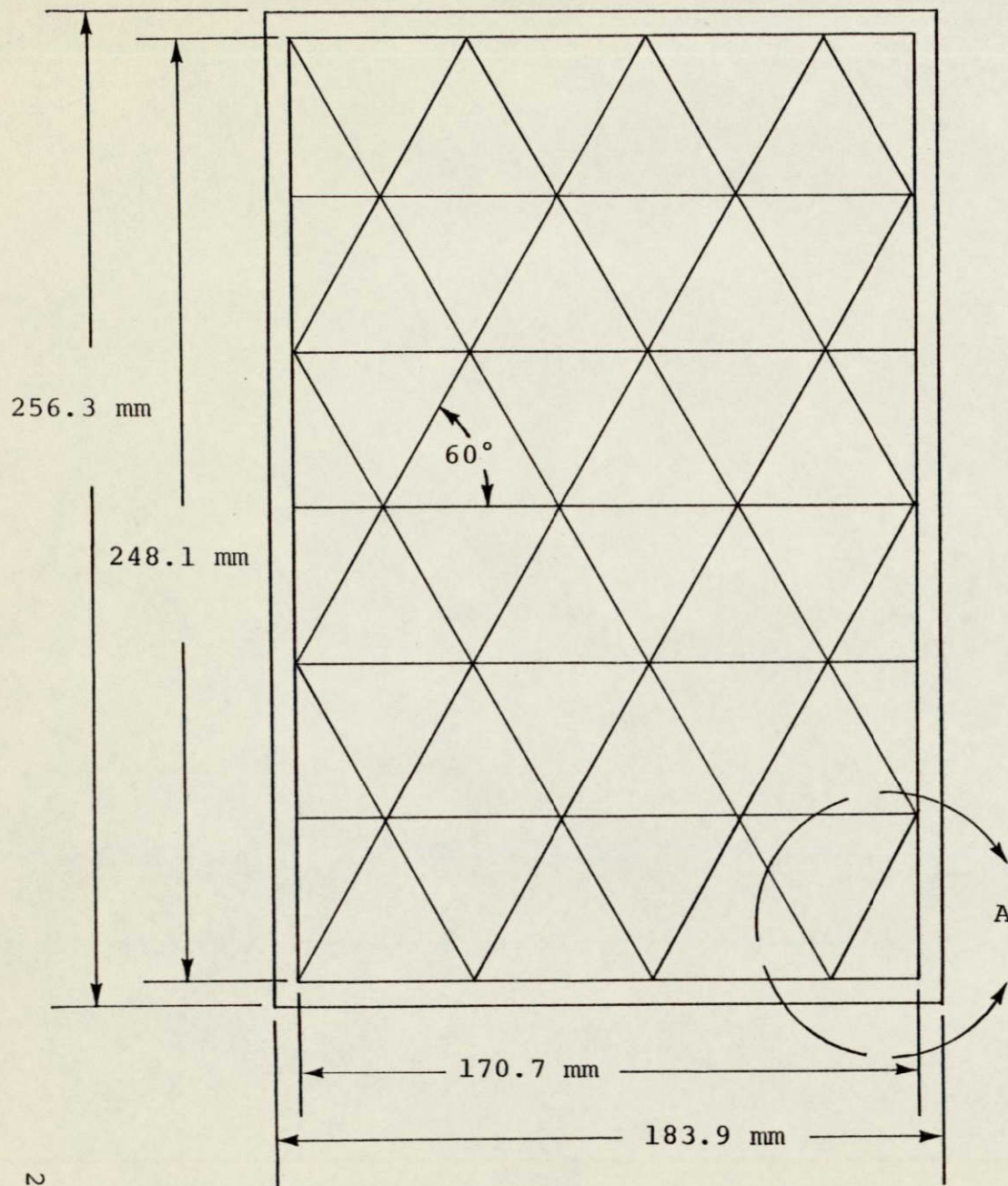
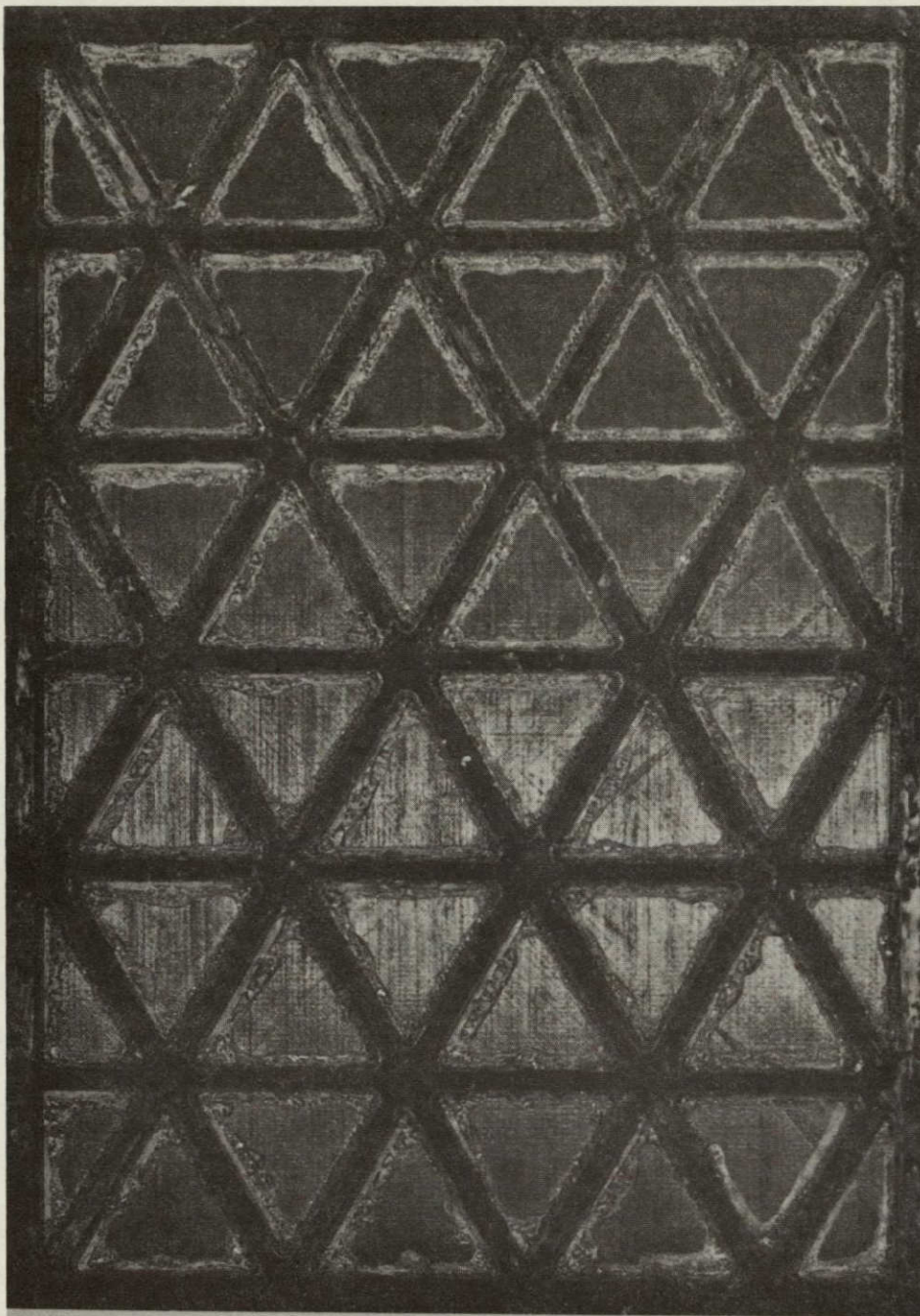


Figure 6. Panel geometry.

ORIGINAL PAGE IS
OF POOR QUALITY



ISOGRID PANEL 9

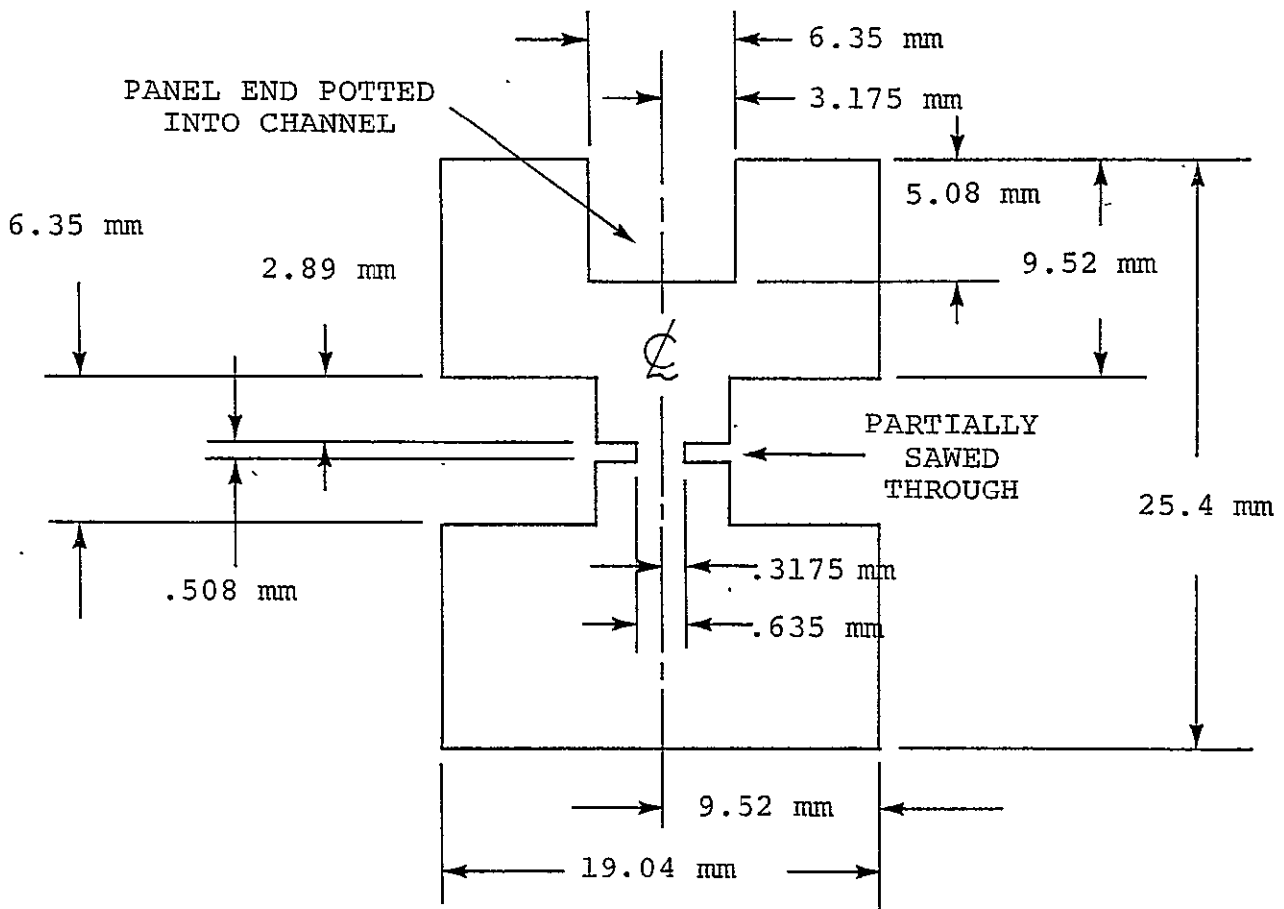
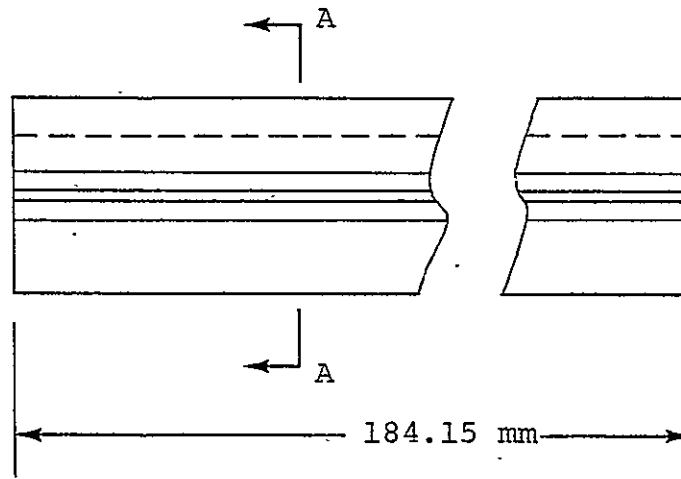


Figure 7. Skin-stiffened panel 9, back view.

ORIGINAL PAGE IS
OF POOR QUALITY



Figure 8. Skin-stiffened panel 9, front view.



SECTION A-A

Figure 9. Top and bottom end fittings.

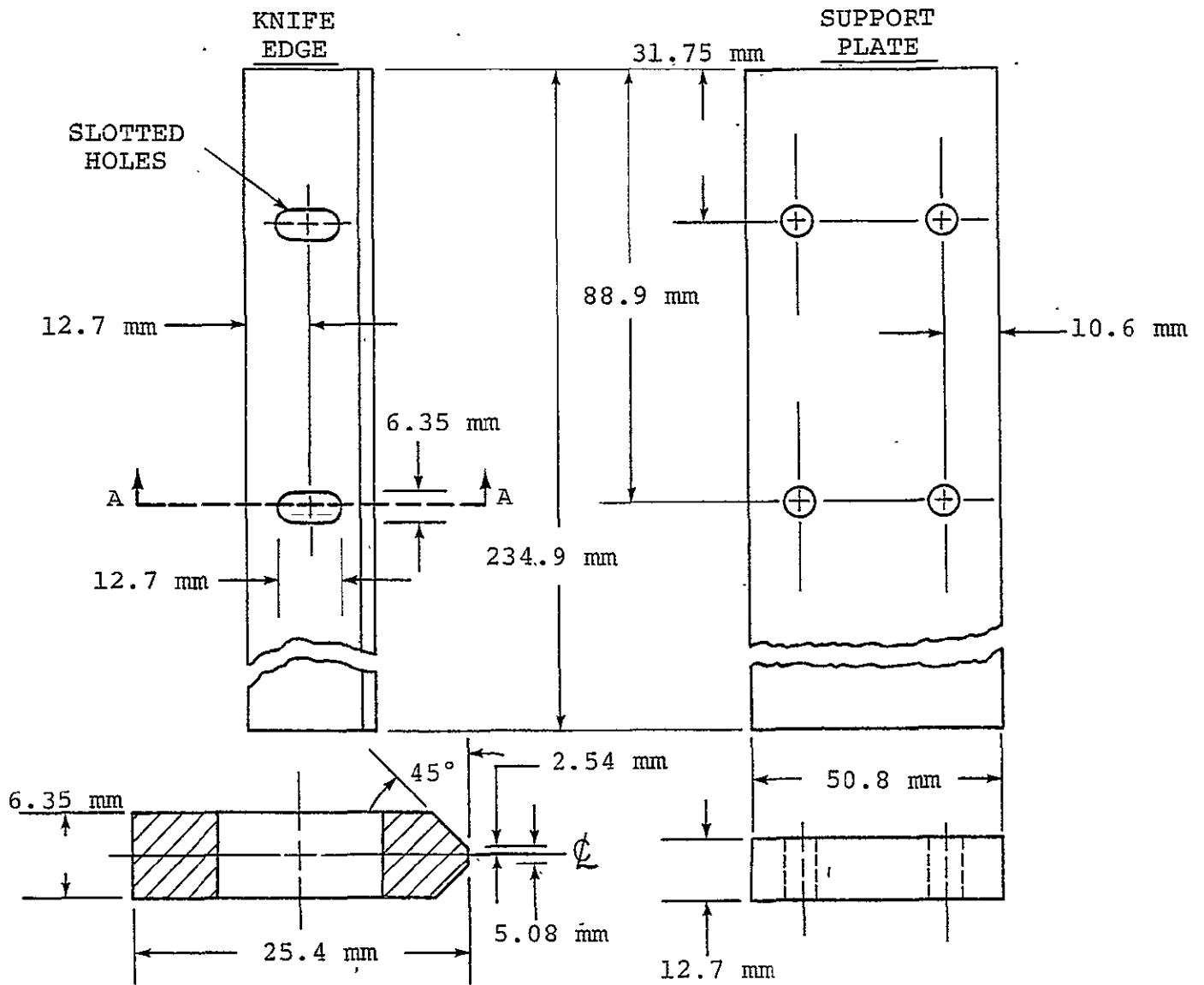
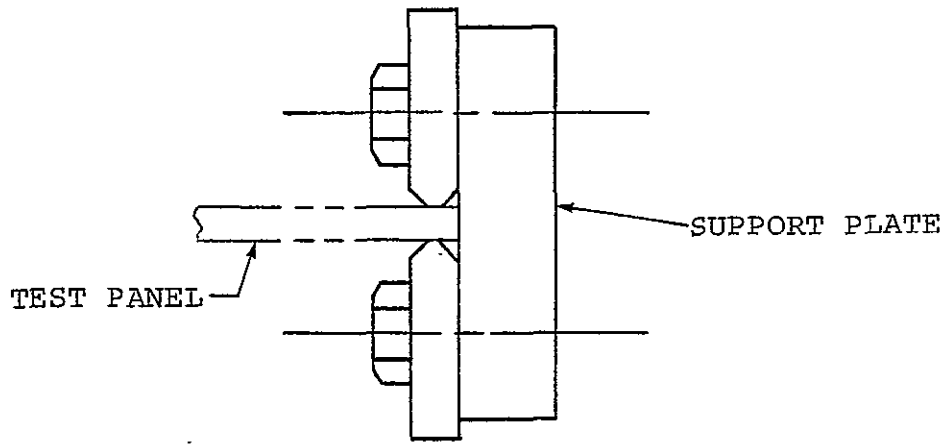
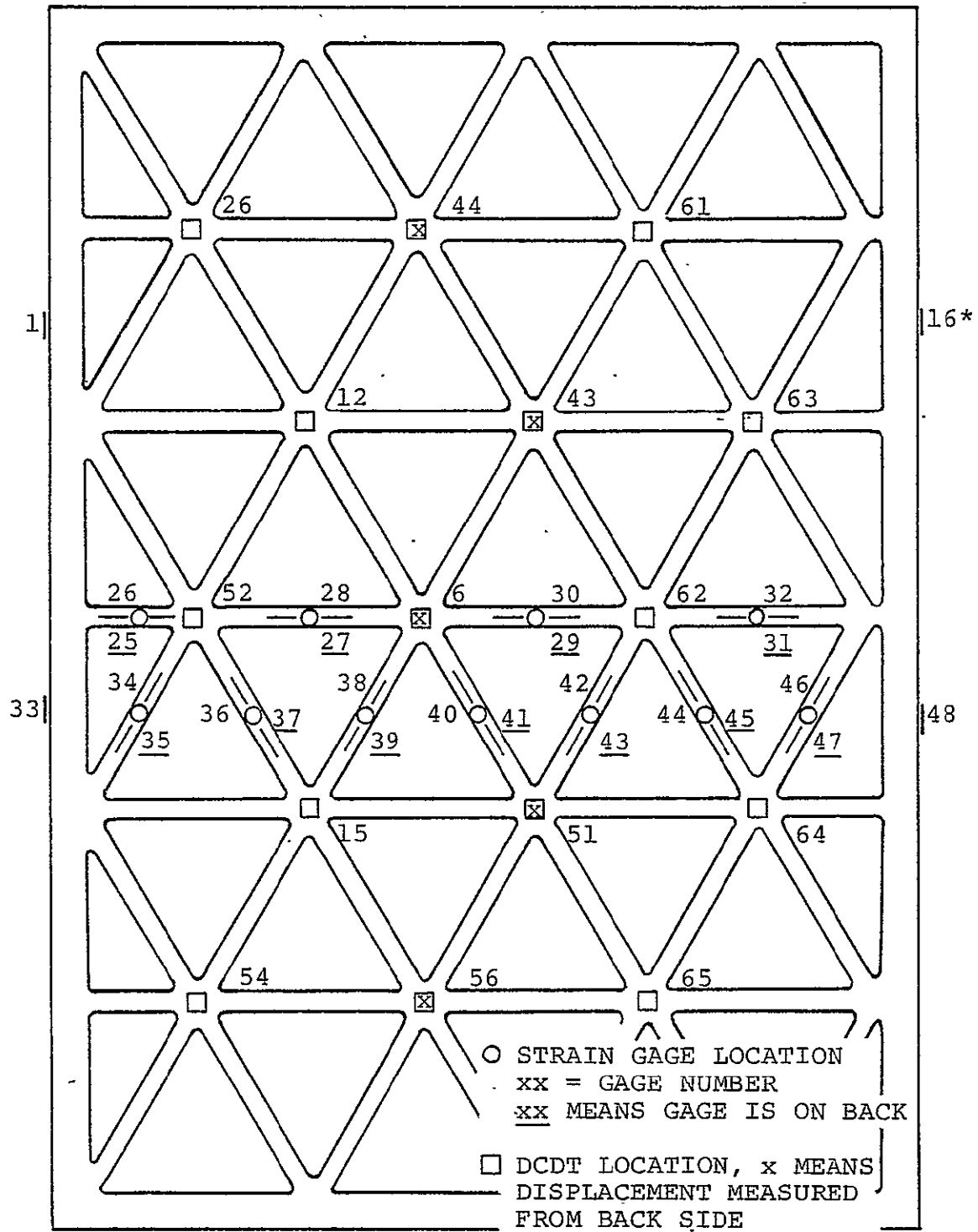


Figure 10. Knife edges for longitudinal side support.



DCDT 55 MEASURED IN-PLANE SHORTENING OF PANEL.

* GAGES 1, 16, 33, 48 ALIGNED AXIALLY ON LONGITUDINAL SIDES.

Figure 11. Strain gage and DCDT location, panel 7.

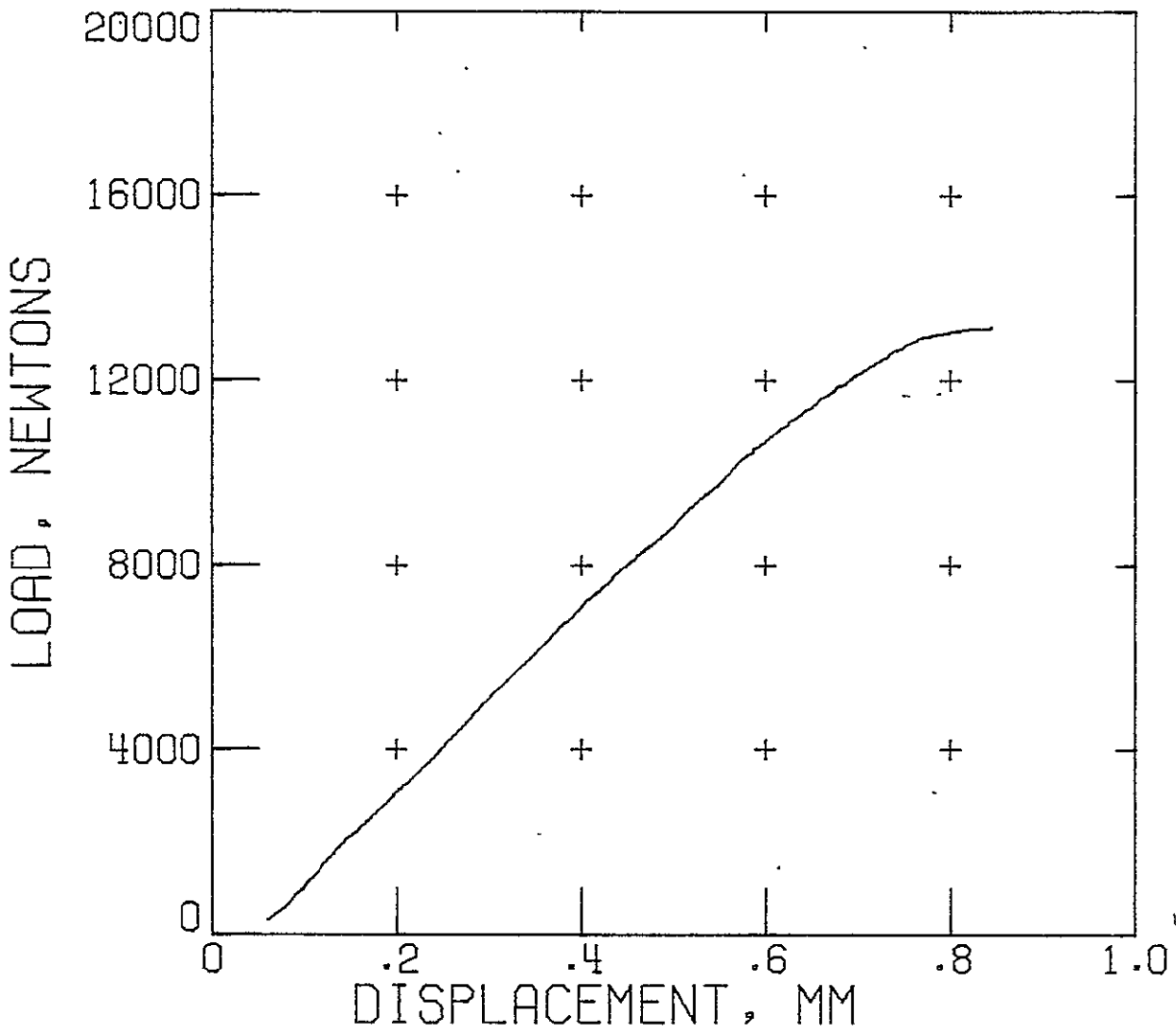


Figure 12. In-plane load-deflection behavior, panel 7.

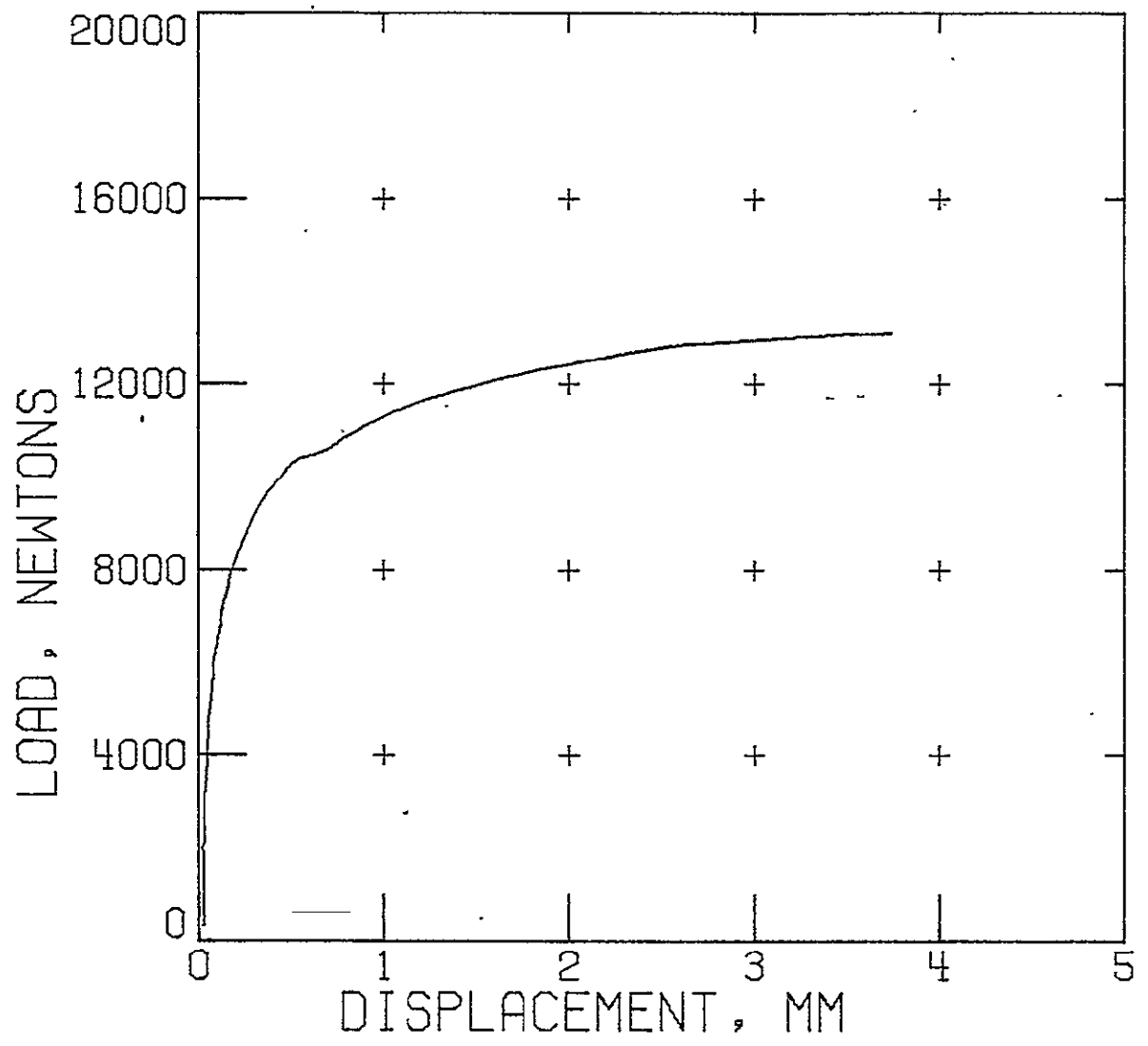


Figure 13. Out-of-plane deflection of node 6, panel 7.

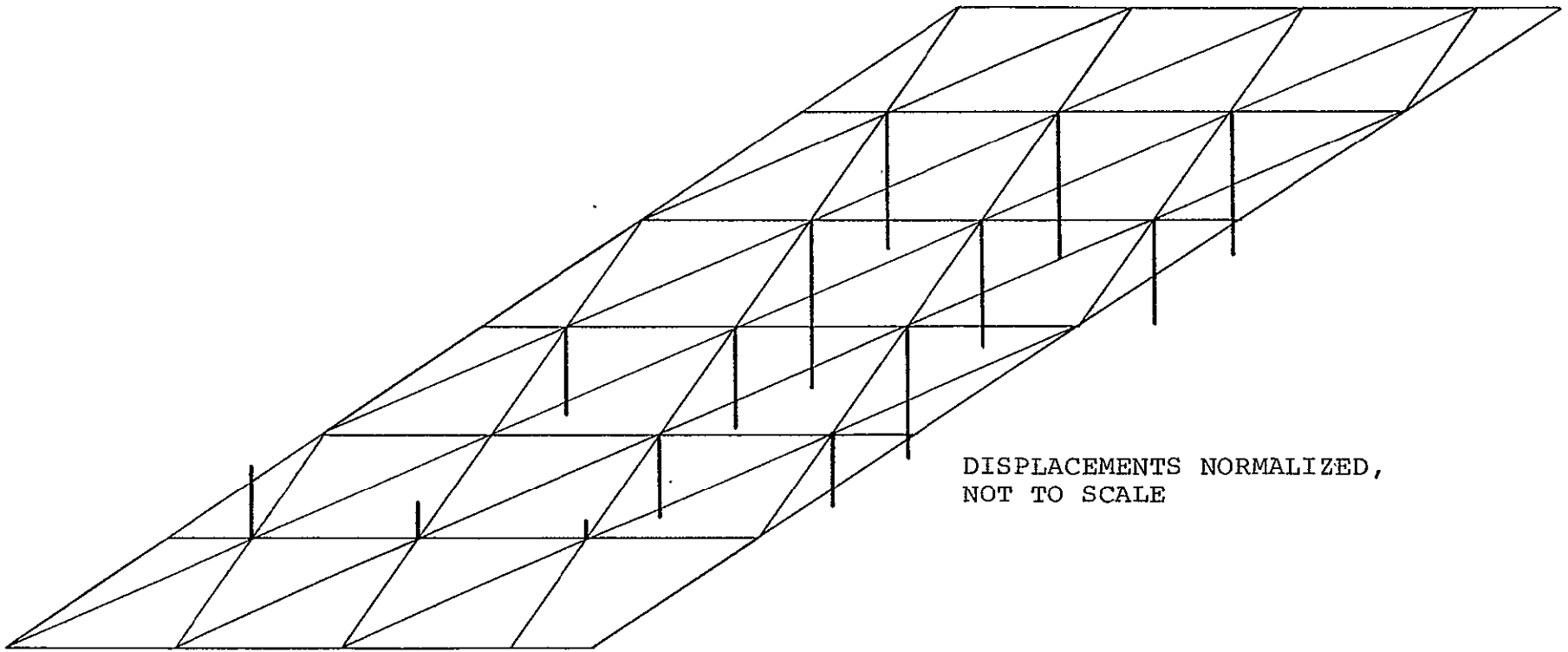


Figure 14. Out-of-plane nodal deflections, panel 7, load = 1808 N.

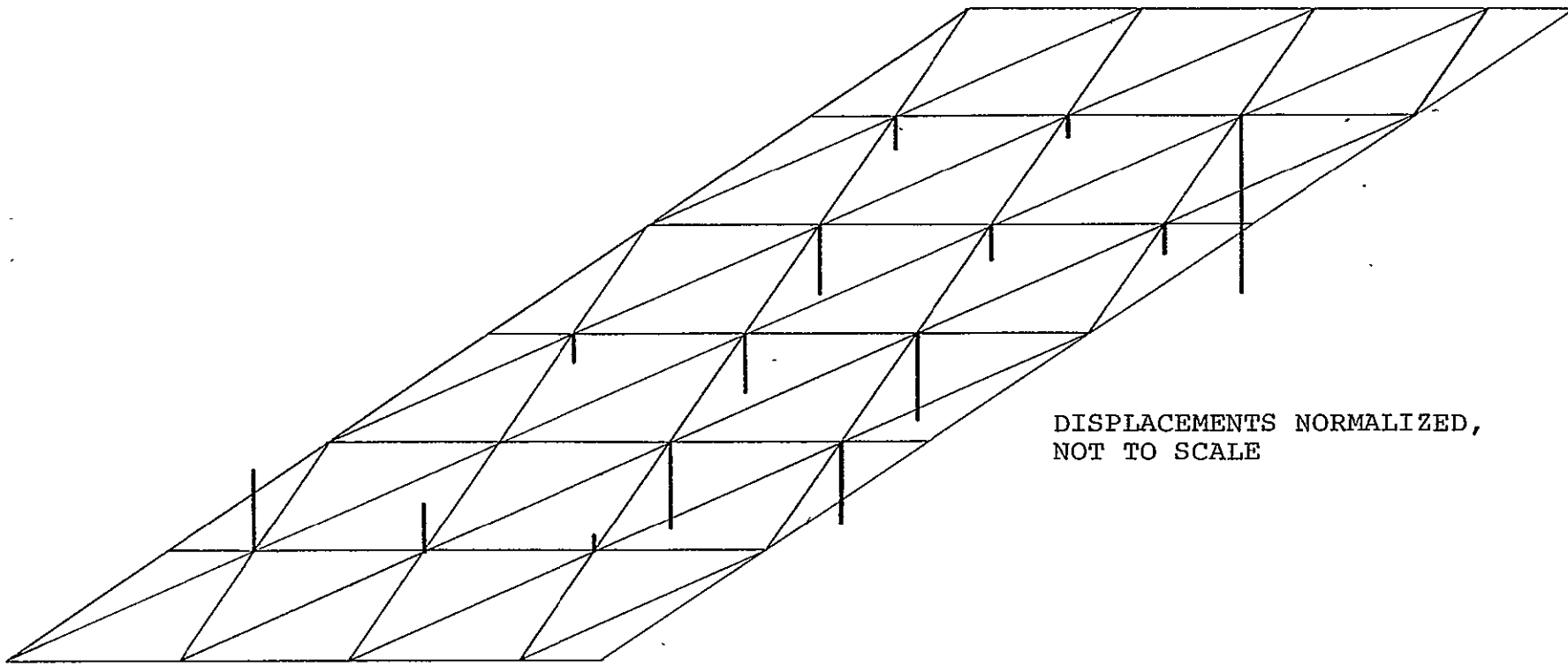


Figure 15. Out-of-plane nodal deflections, panel 7, load = 6142 N.

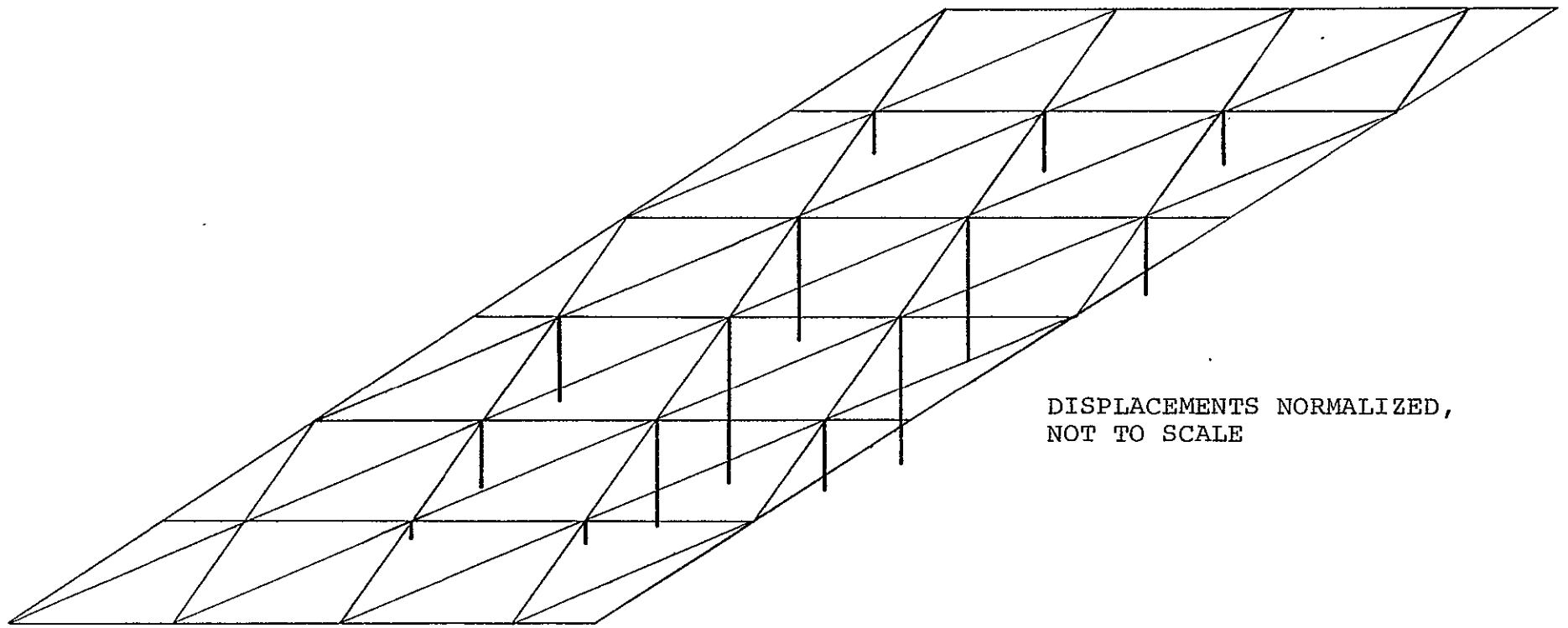


Figure 16. Out-of-plane nodal deflections, panel 7, load = 12751 N.

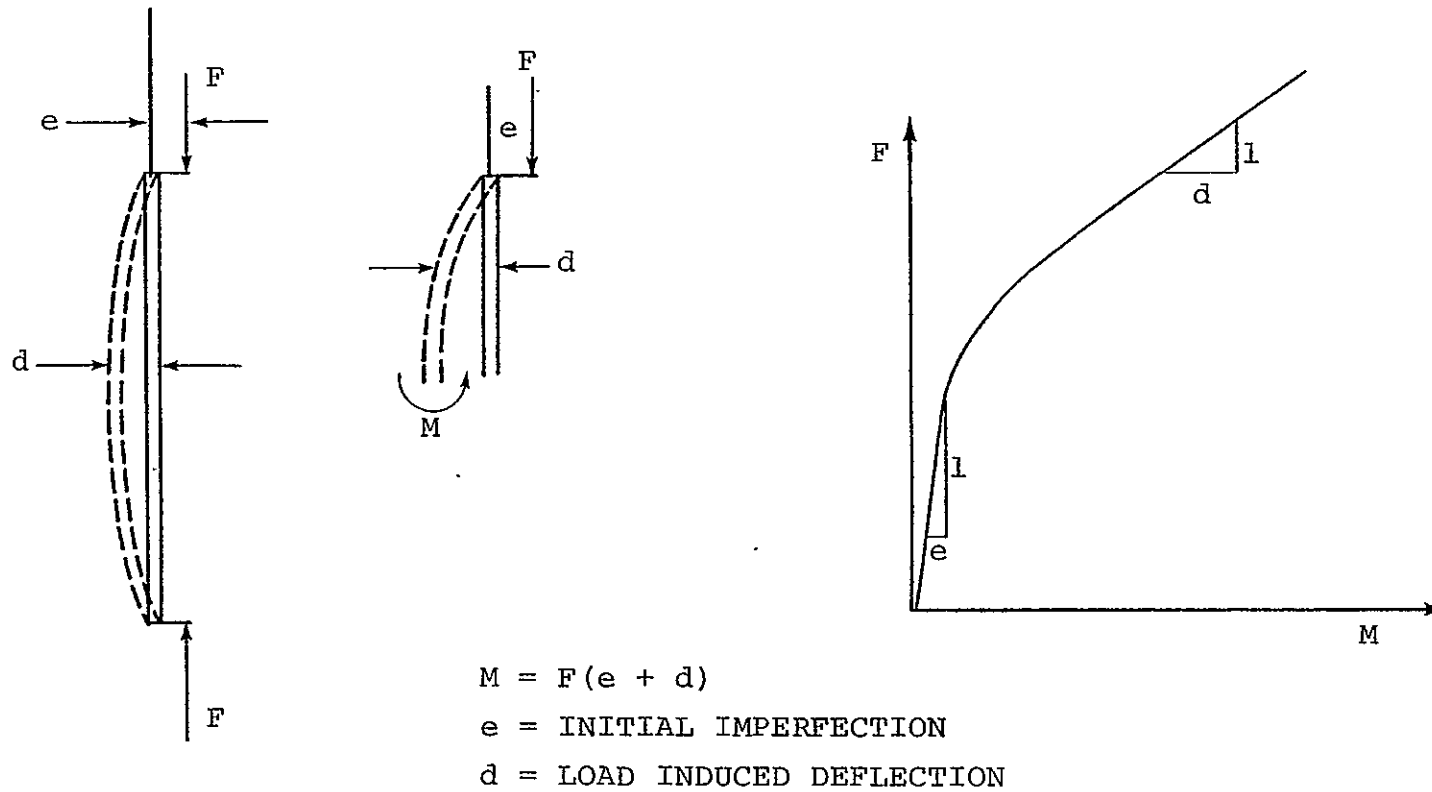


Figure 17. Effect of initial imperfection on force versus moment for a beam-column.

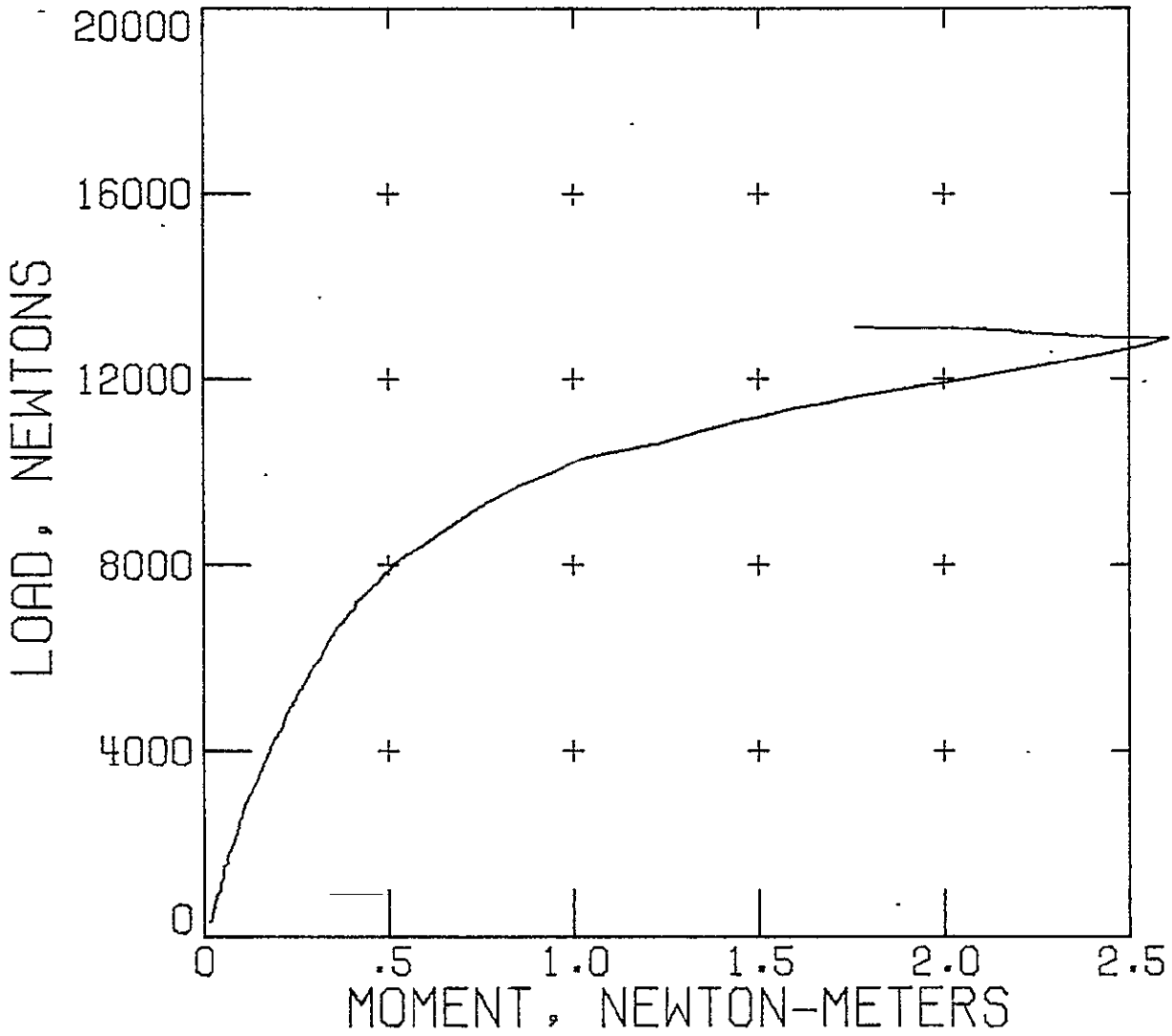


Figure 18. Force versus moment across gaged section of panel 7.

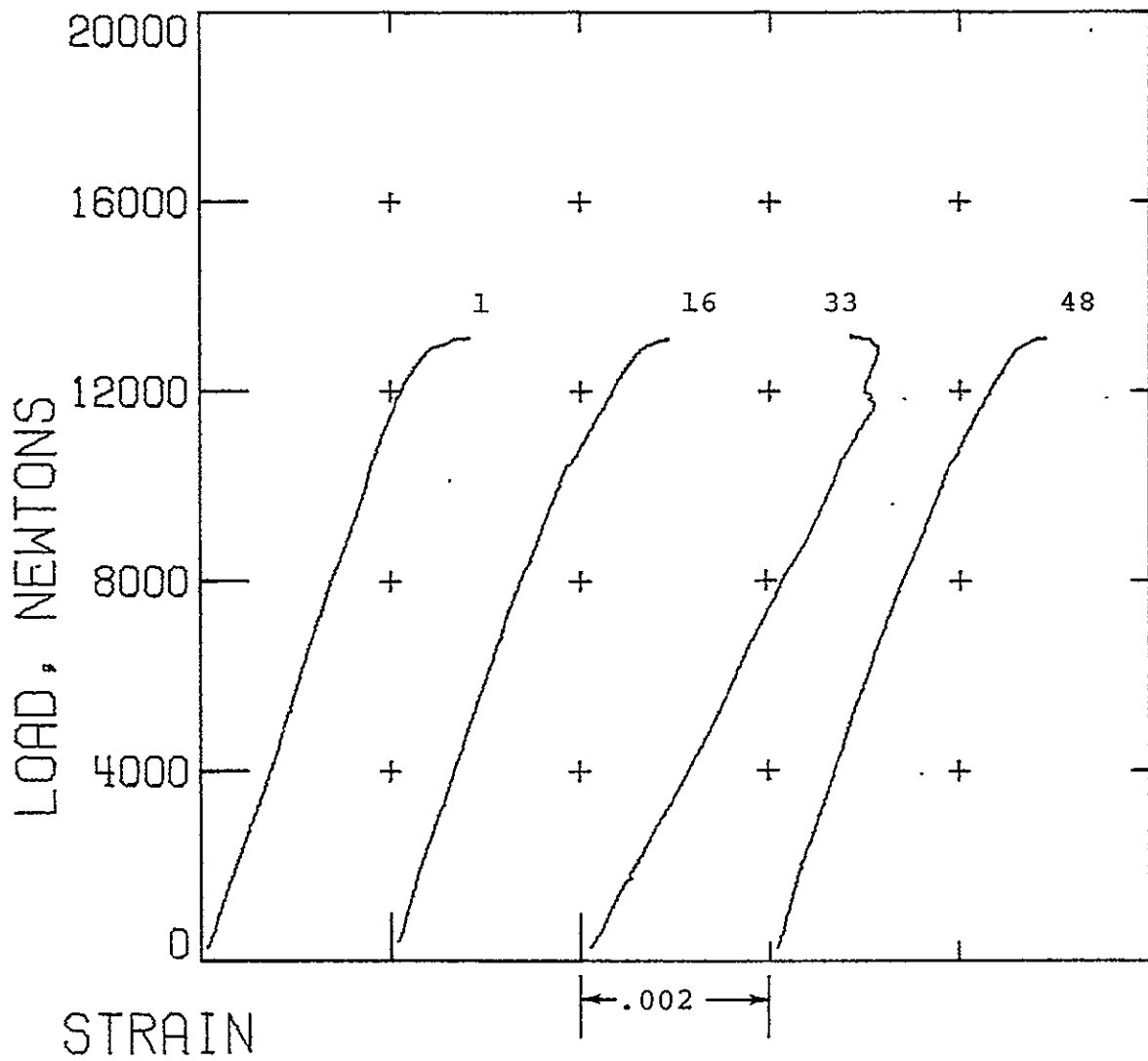
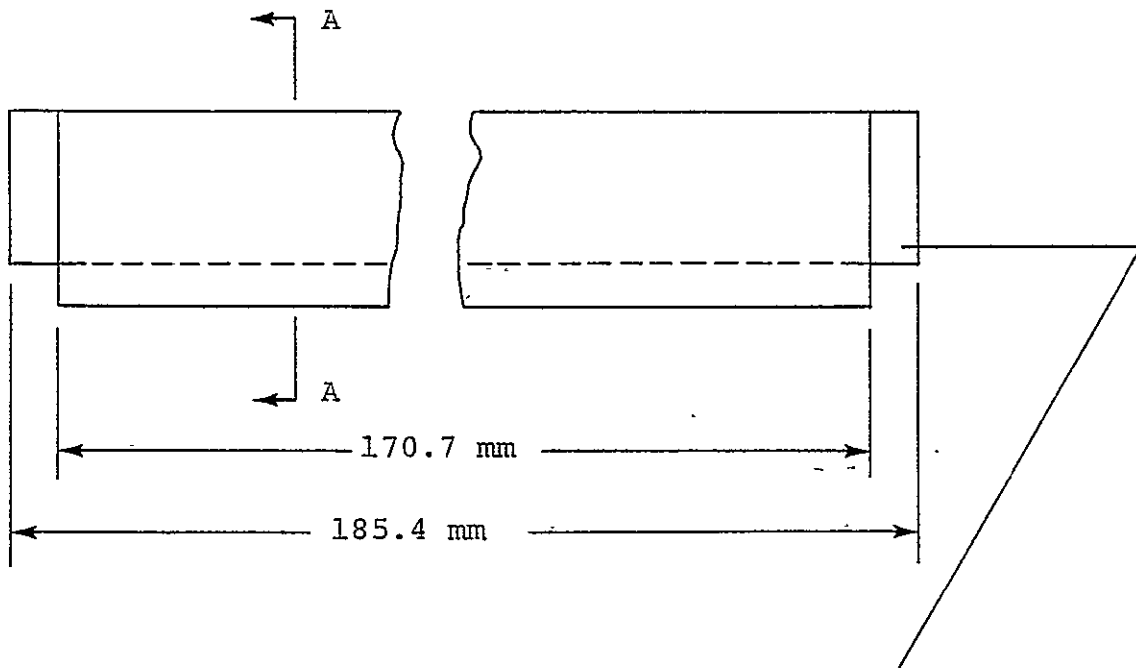
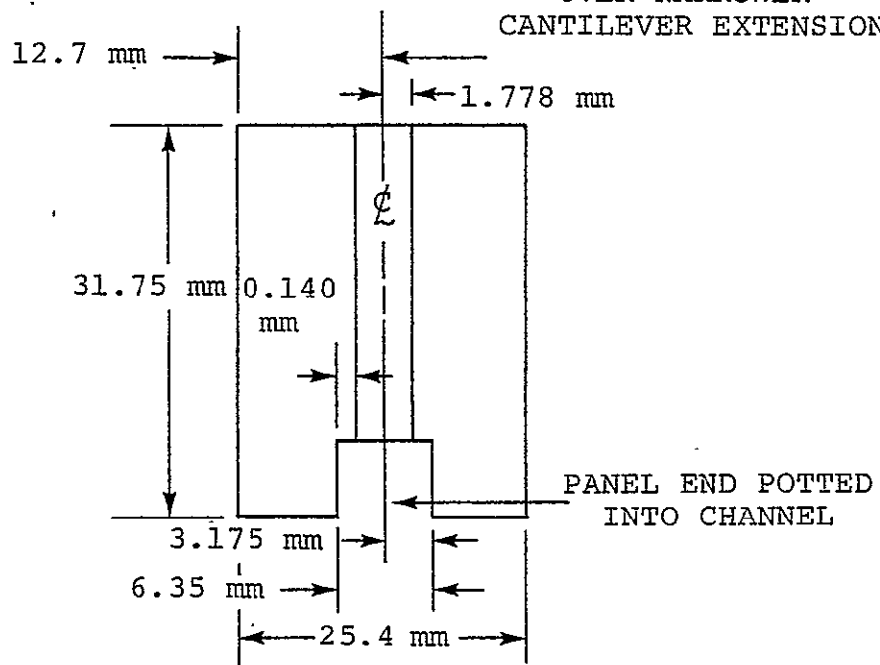


Figure 19. Strain versus force for gages 1, 16, 33, and 48 on panel 7.

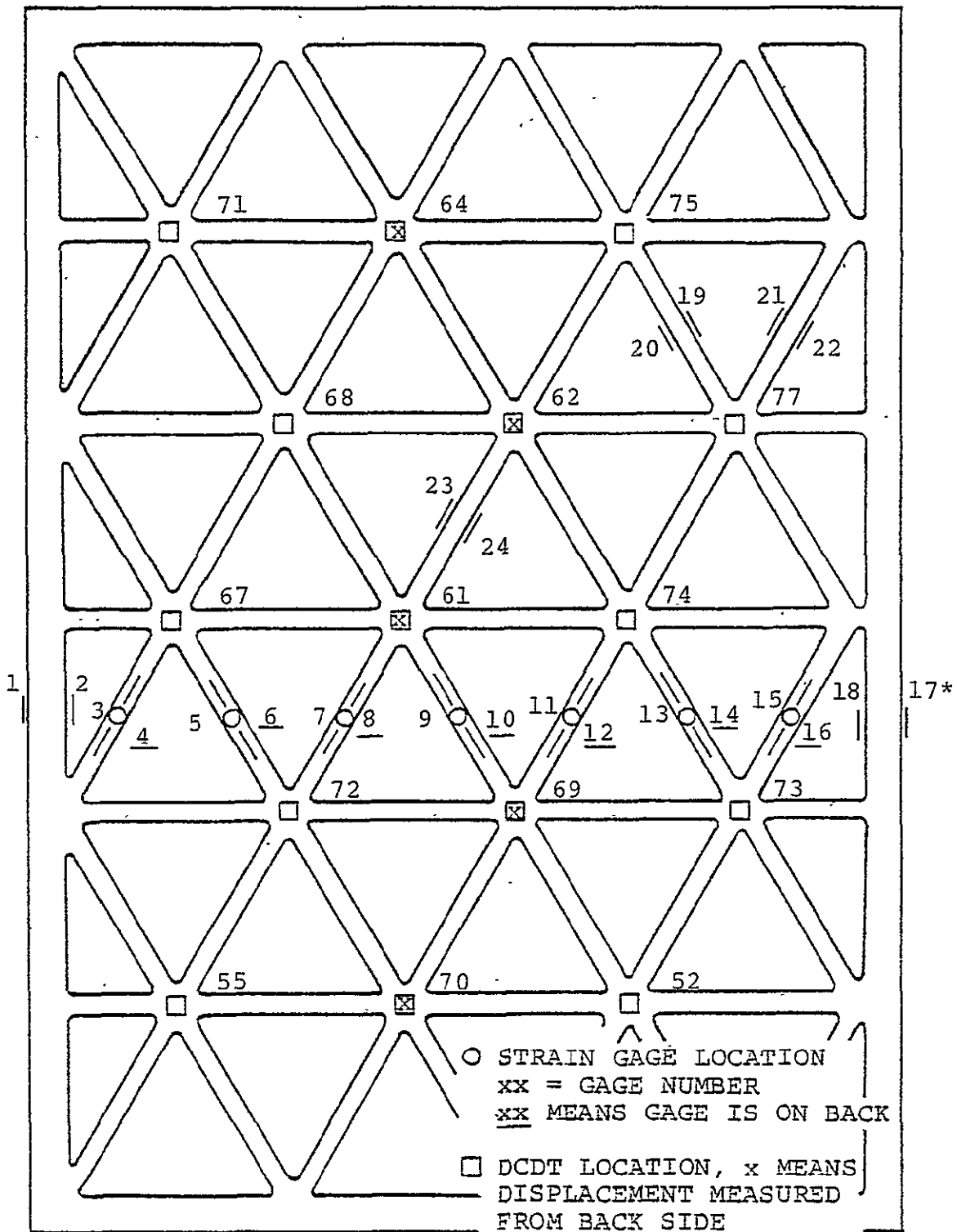


KNIFE EDGE EXTENDS
OVER NARROWER
CANTILEVER EXTENSION



SECTION A-A

Figure 20. Modified end fittings for panel 8.



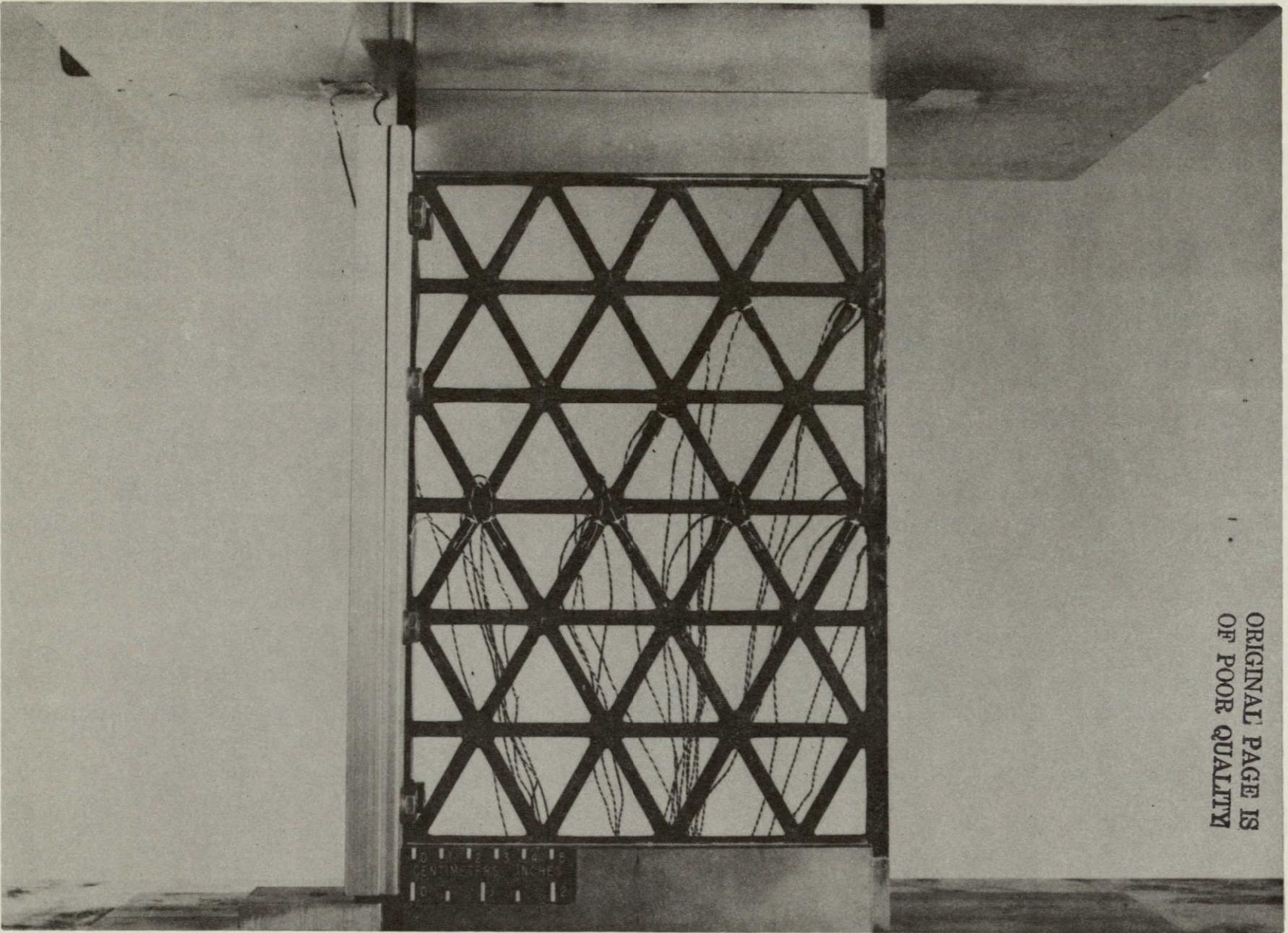
DCDT 65 MEASURED IN-PLANE SHORTENING OF PANEL.

* GAGES 1, 2, 17, 18, 19, 20, 21, 22, 23, 24 ALIGNED AXIALLY ALONG LEGS OF GRID OR ON LONGITUDINAL SIDES.

Figure 21. Strain gage and DCDT location, panel 8.

ORIGINAL PAGE IS
 OF POOR QUALITY

ORIGINAL PAGE IS
 OF POOR QUALITY



ORIGINAL PAGE IS
OF POOR QUALITY

Figure 22. Panel 8 in test fixture.

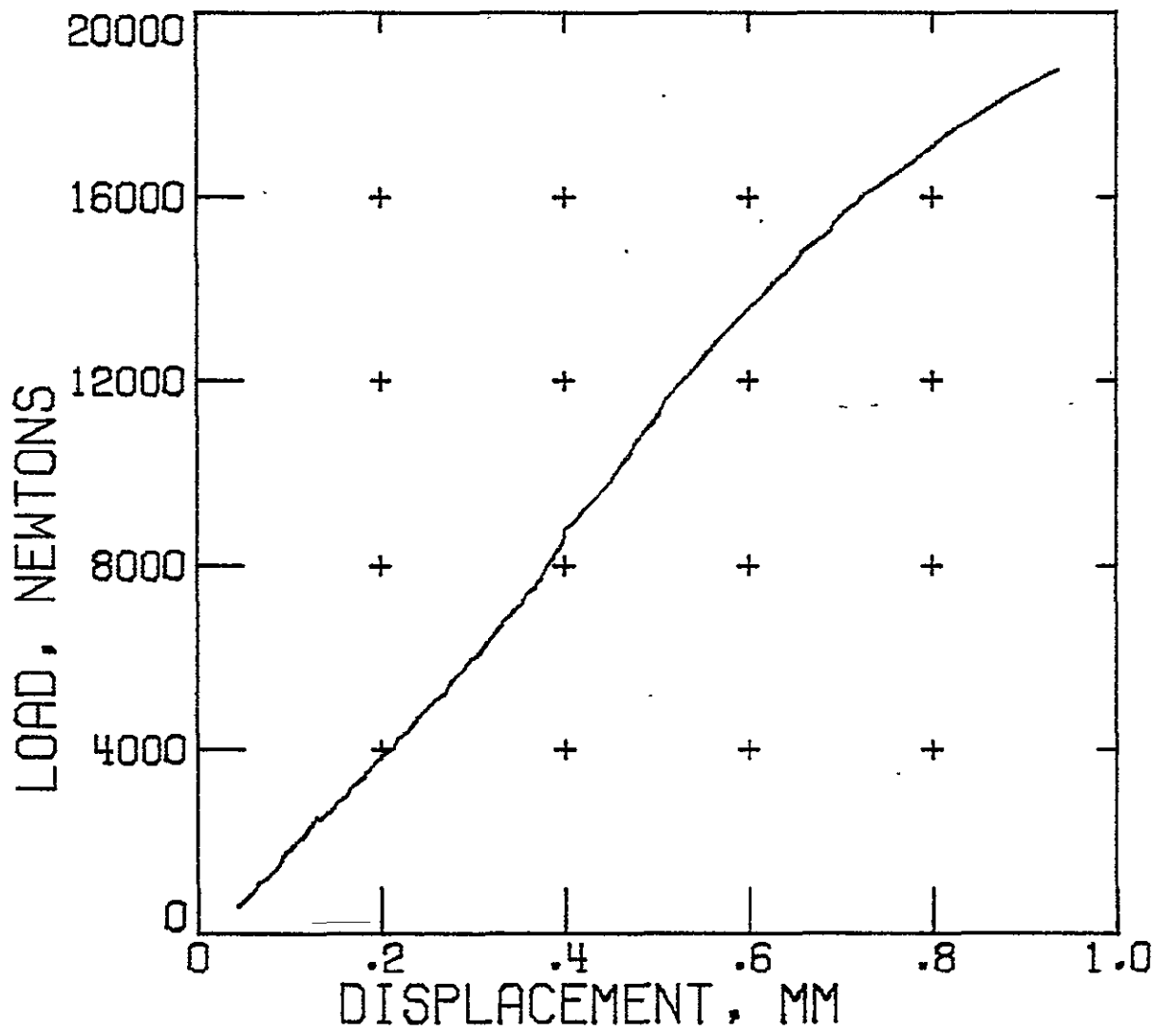


Figure 23. In-plane load-deflection behavior of panel 8.

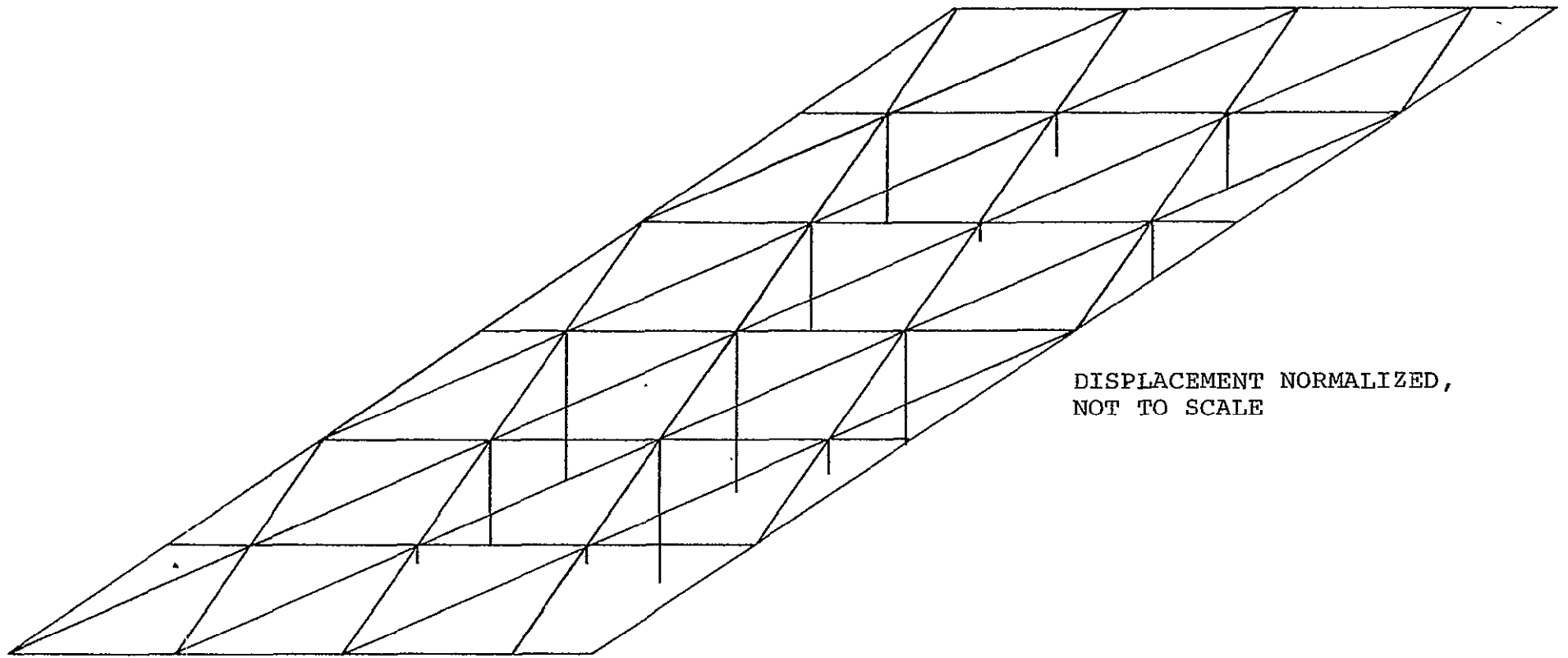


Figure 24. Out-of-plane nodal deflections, panel 8, load = 1860 N.

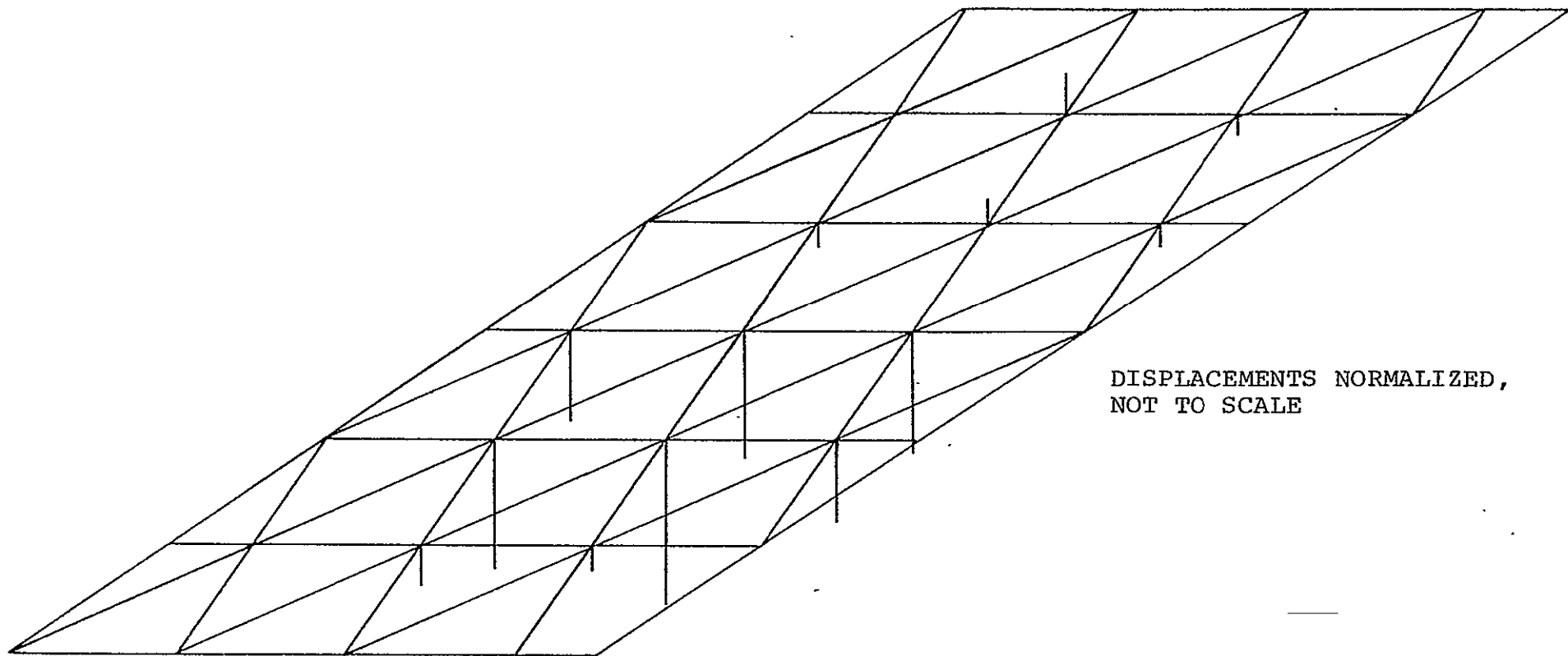


Figure 25. Out-of-plane nodal deflections, panel 8, load = 6212 N.

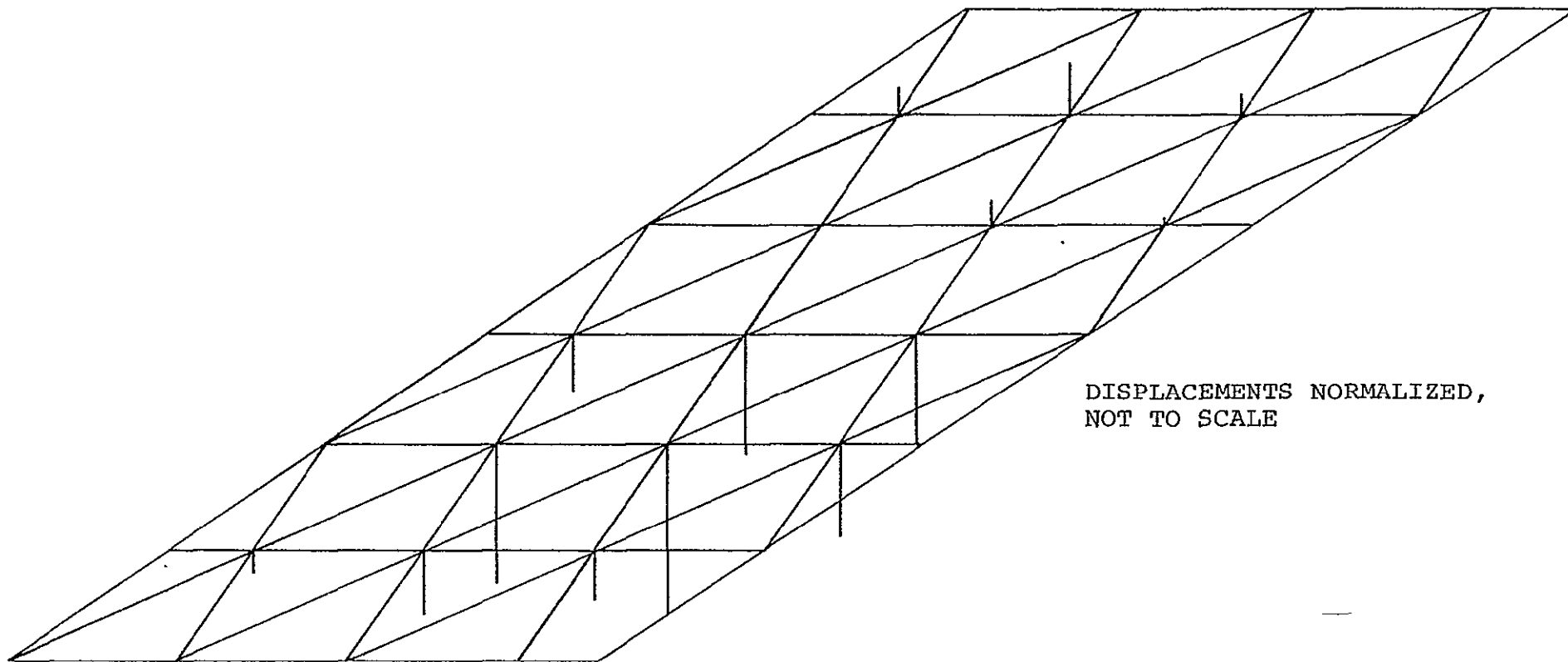


Figure 26. Out-of-plane nodal deflections, panel 8, load = 13065 N.

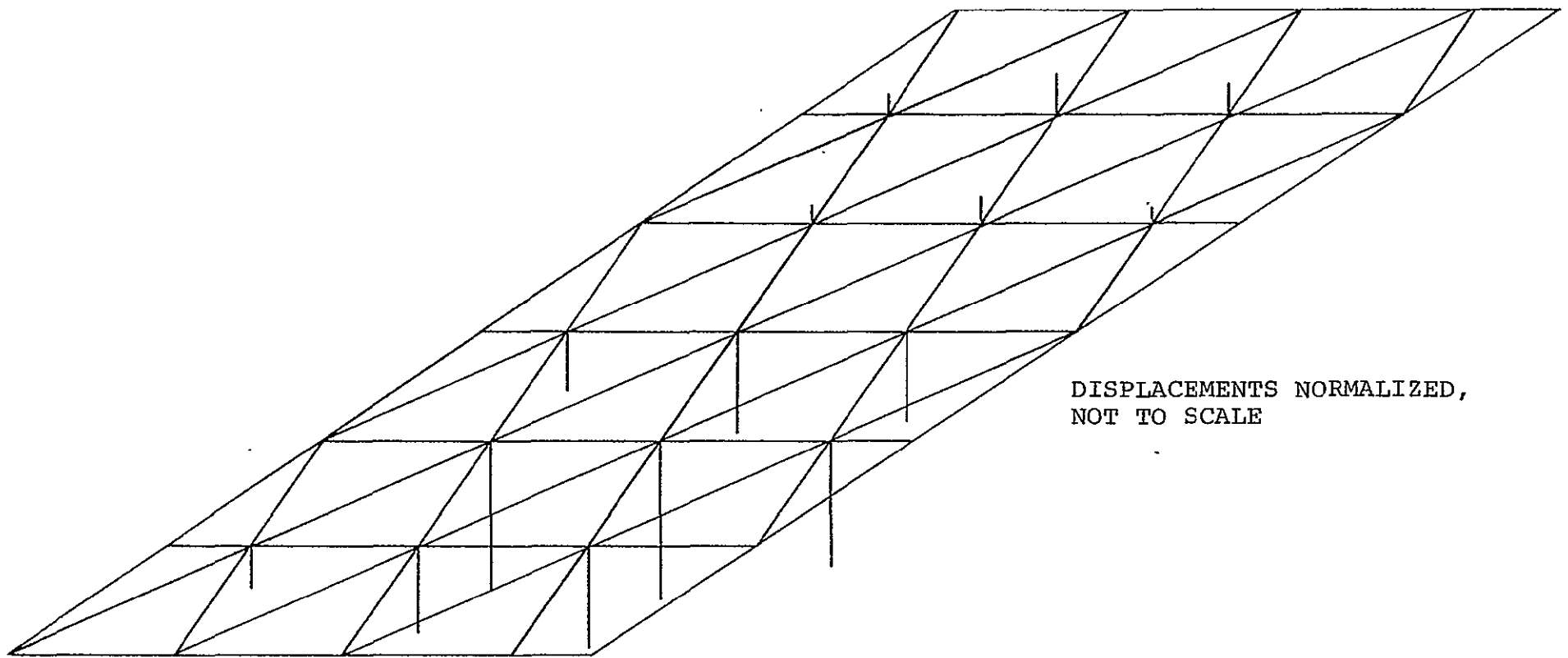


Figure 27. Out-of-plane nodal deflections, panel 8, load = 18766 N.

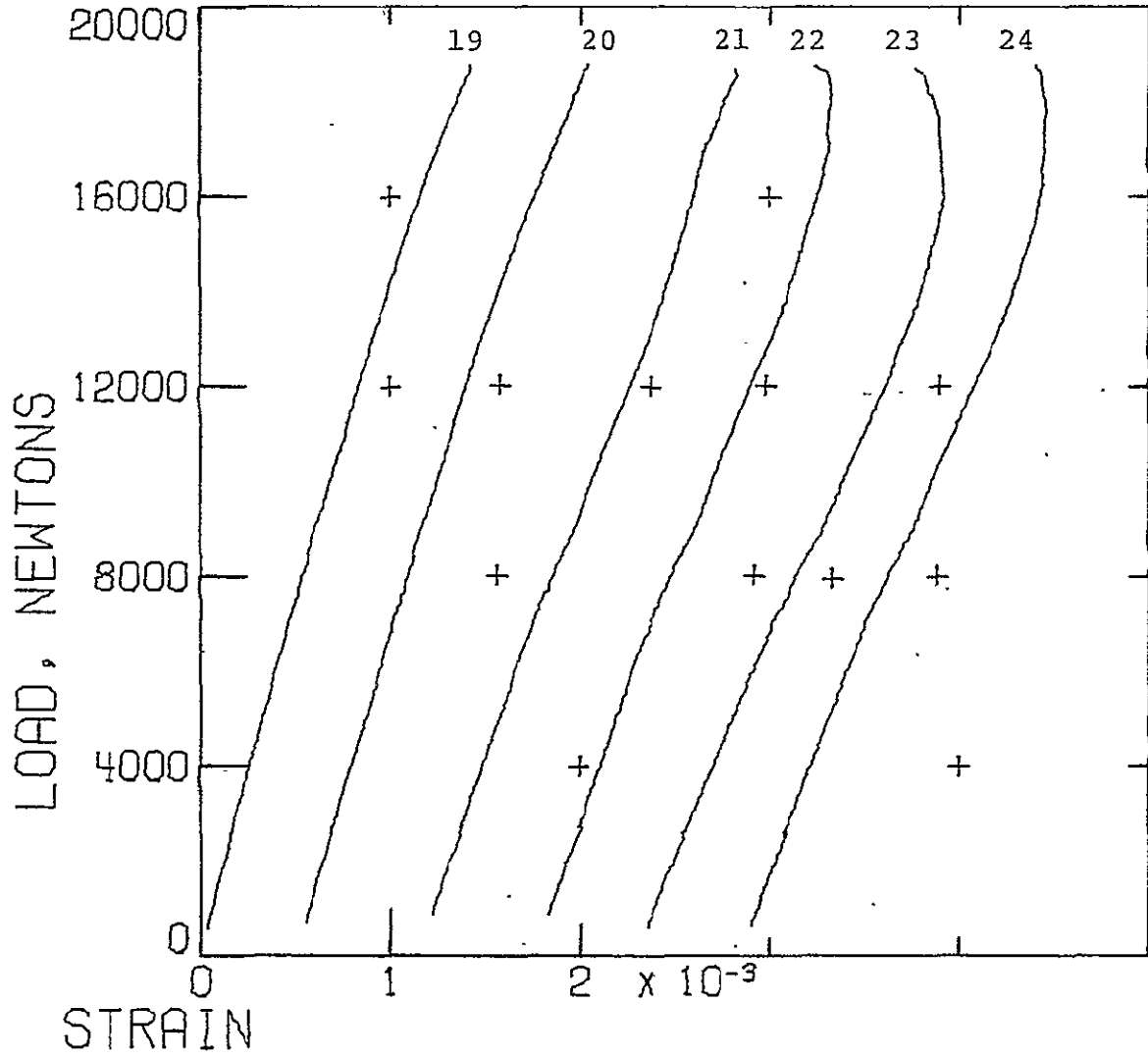


Figure 28. Strain versus load for back-to-back gage pairs 19-20, 21-22, and 23-24.

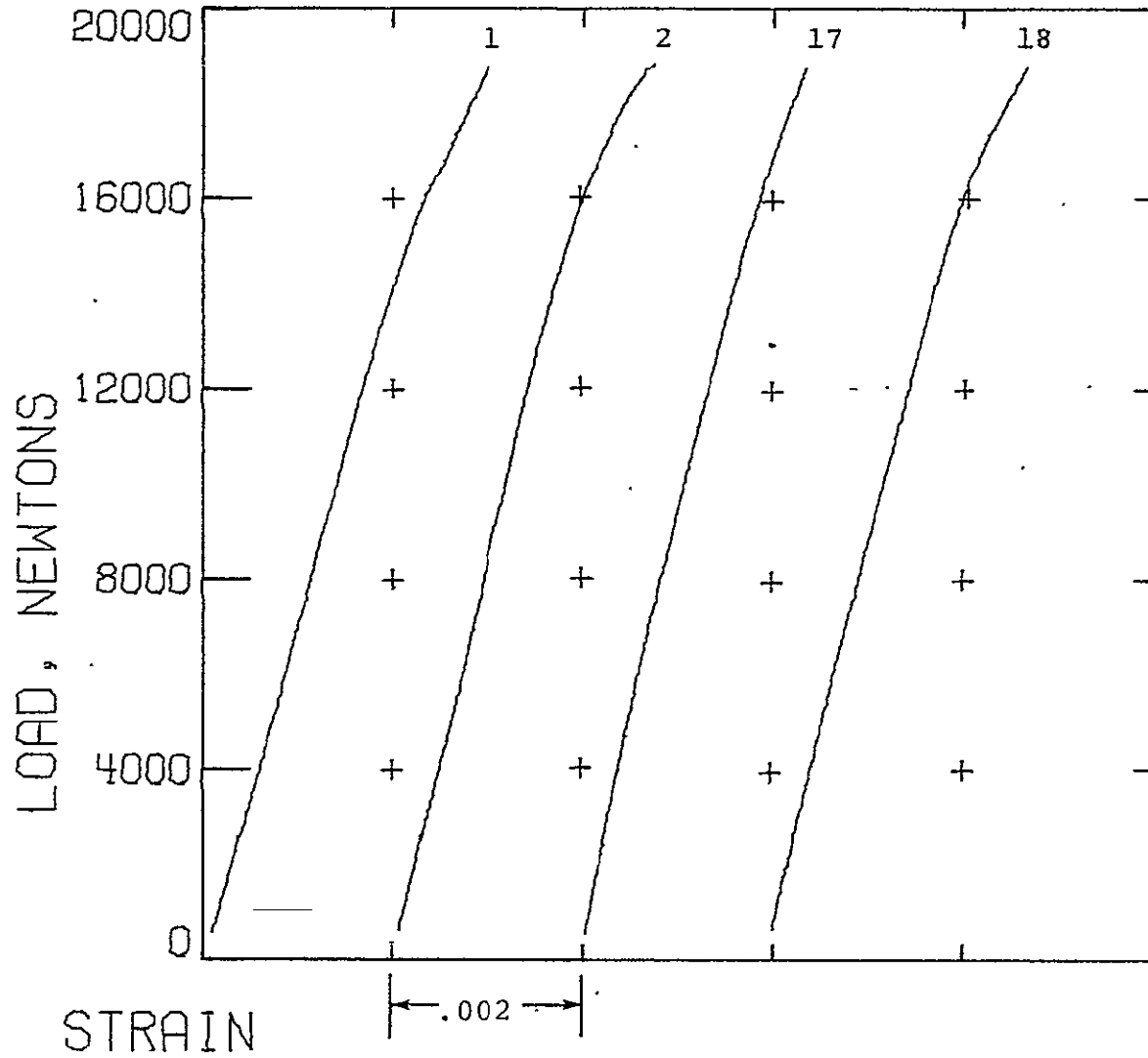
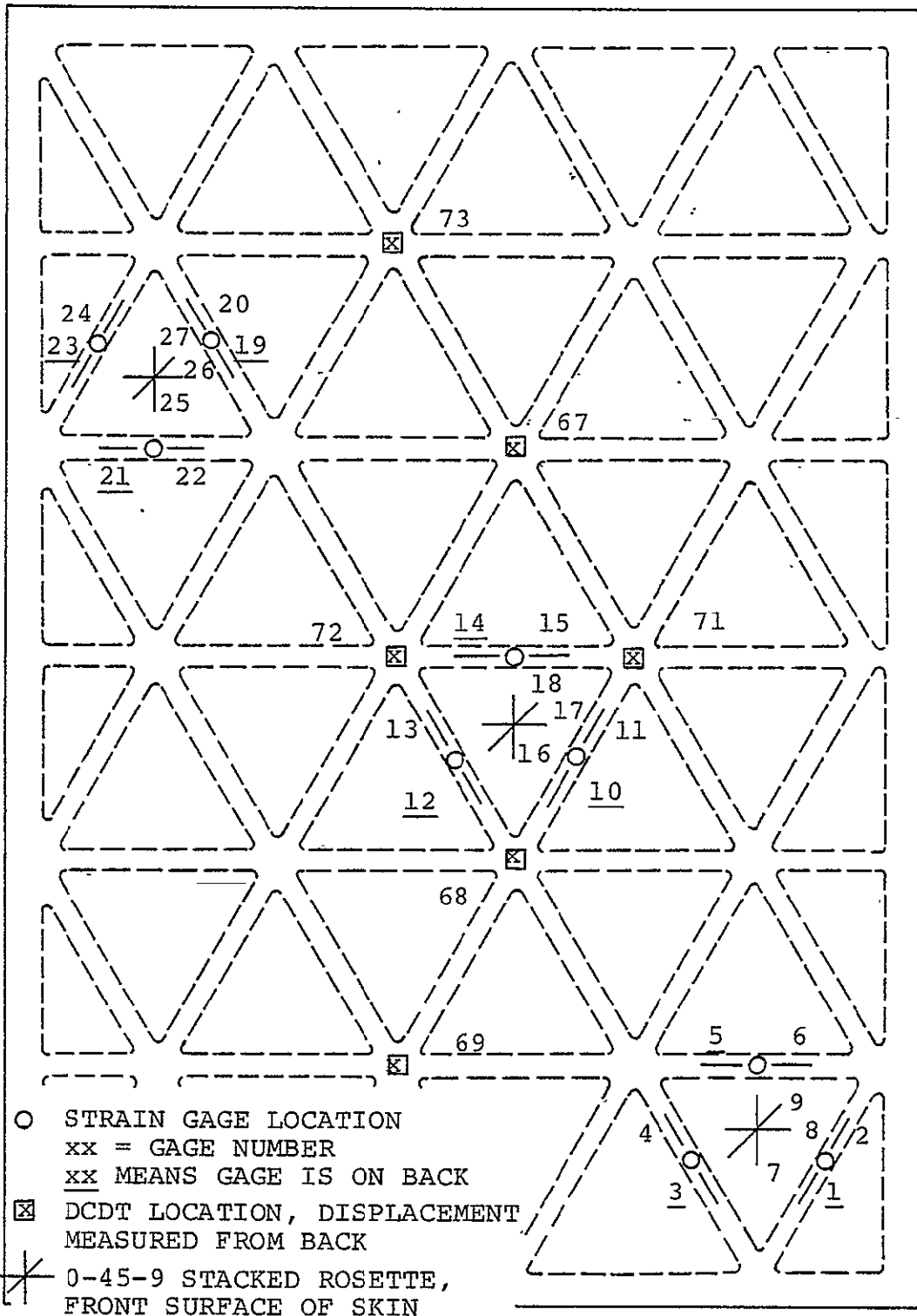


Figure 29. Strain versus load for back-to-back gage pairs 1-2 and 17-18.



DCDT 75 MEASURES IN-PLANE SHORTENING OF PANEL.

Figure 30. Strain gage and DCDT locations, panel 9.

ORIGINAL PAGE IS
OF POOR QUALITY

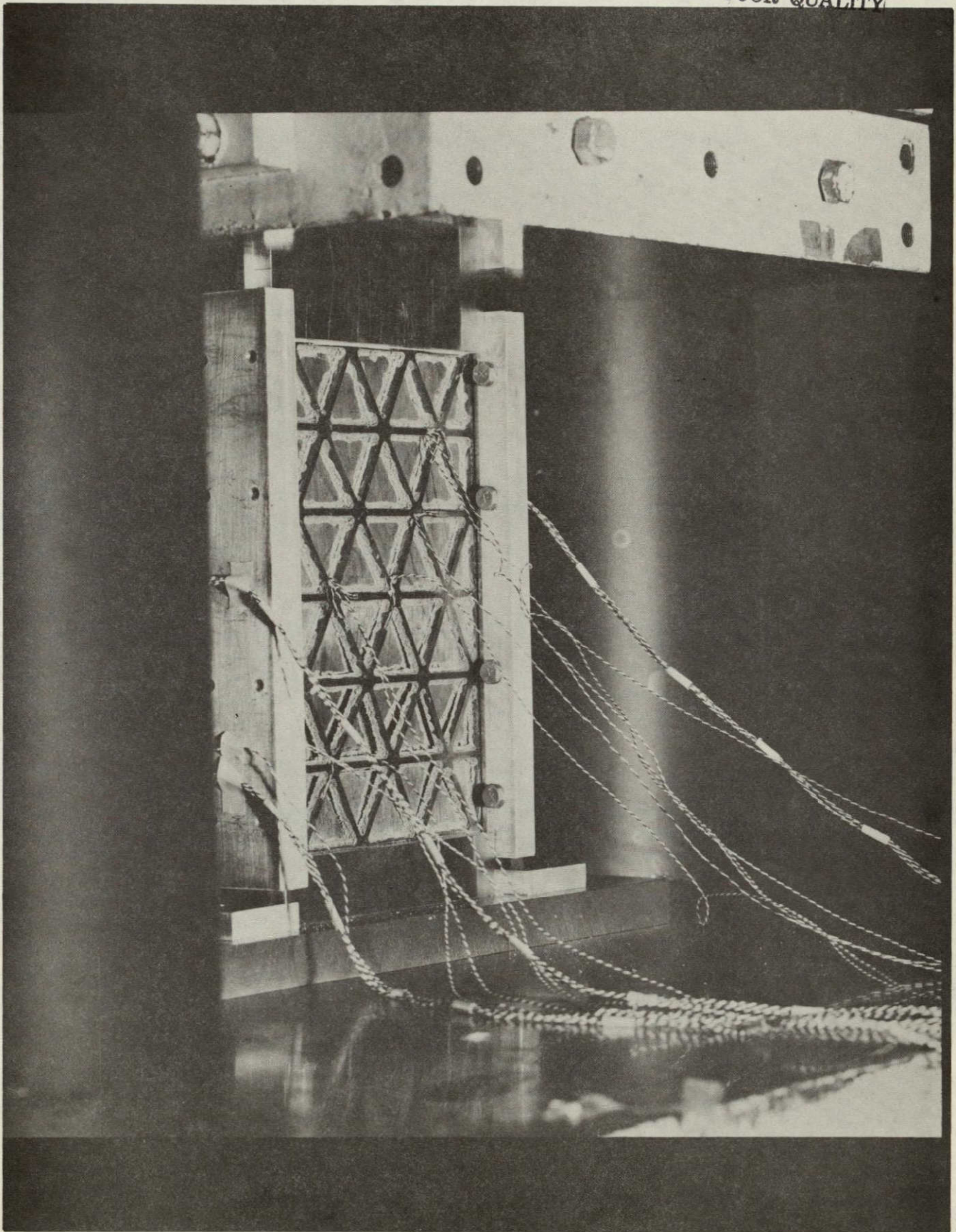


Figure 31. Separation of skin and framework on skin-stiffened panel.

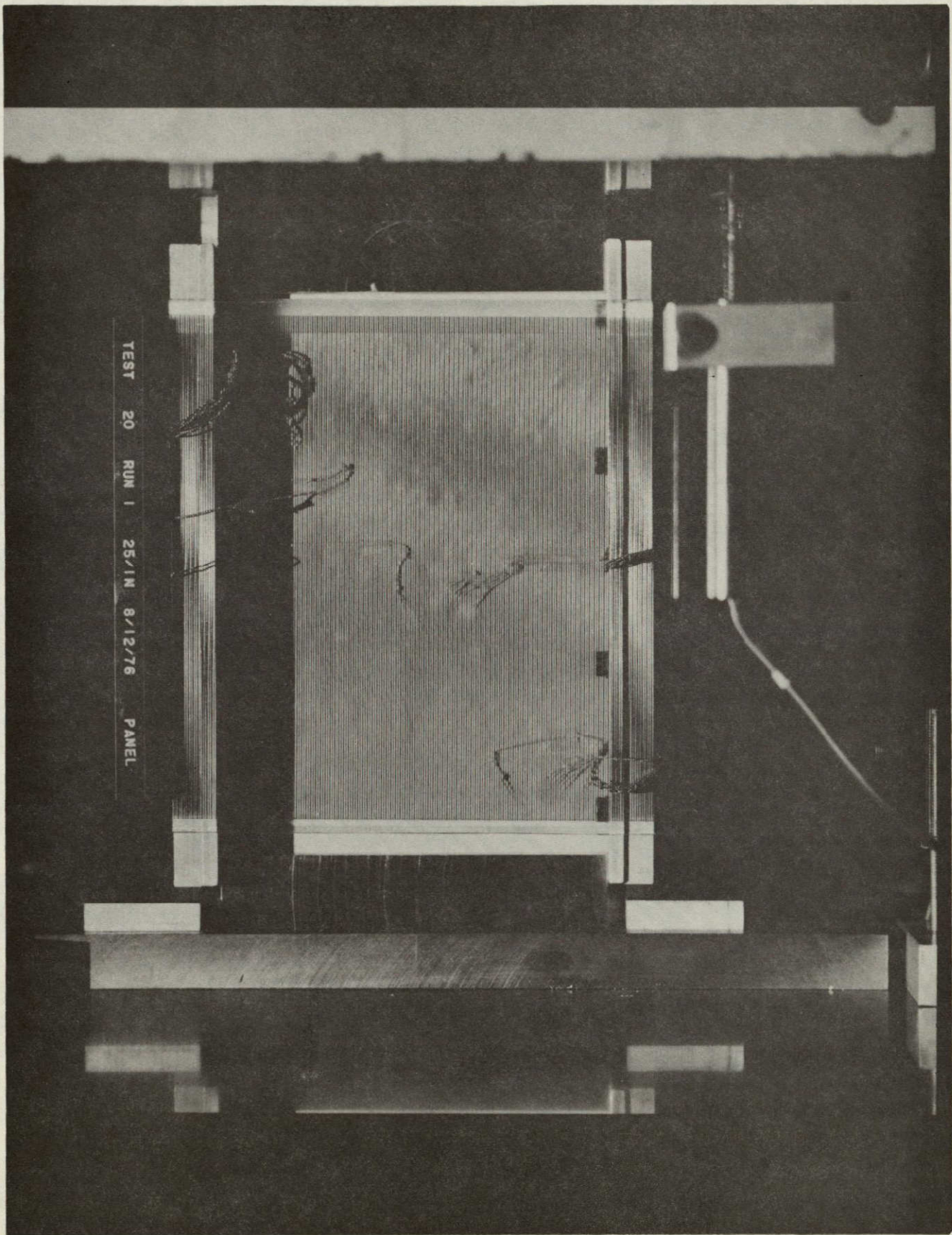


Figure 32. Moiré fringe pattern on panel 9 at no-load condition.

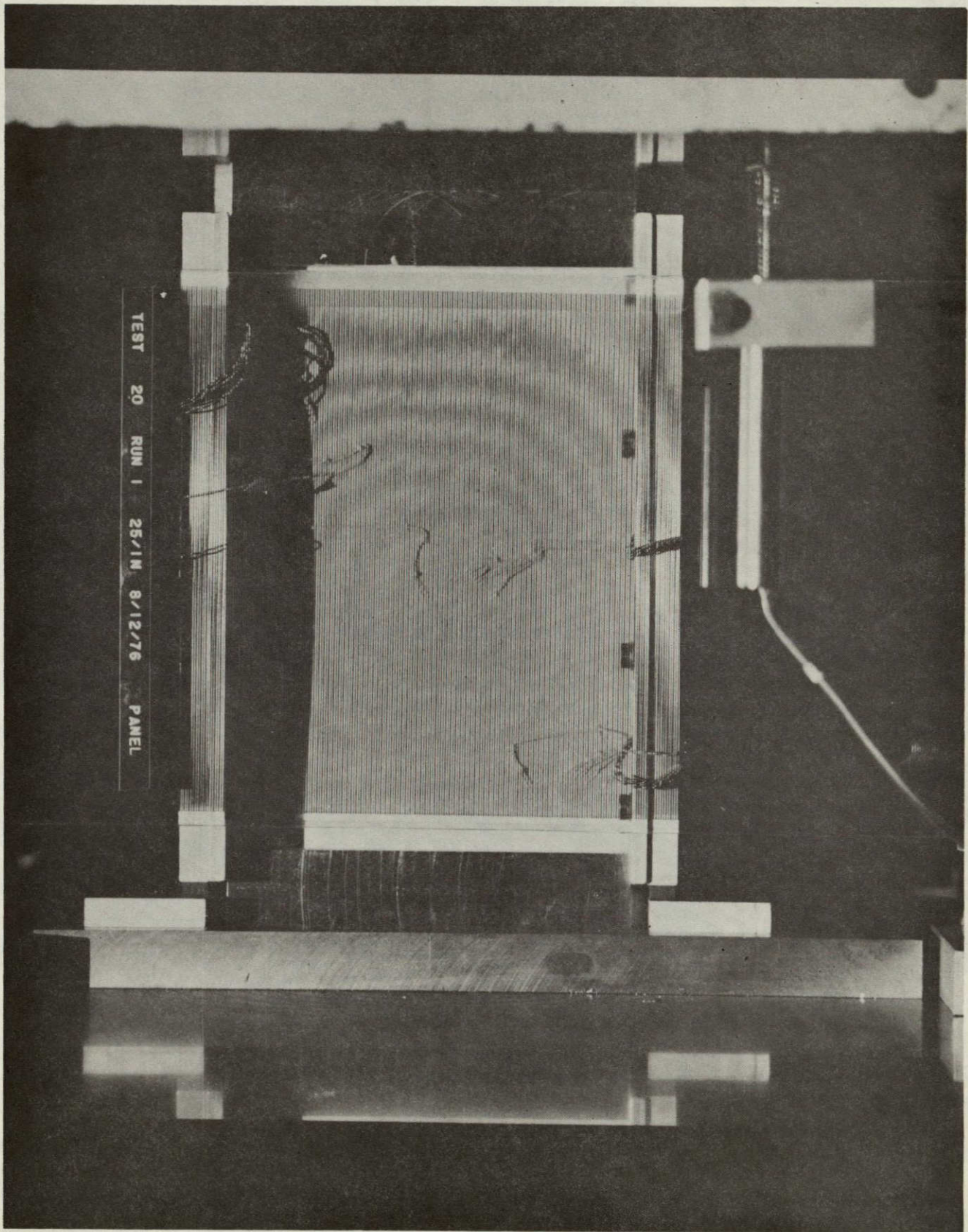


Figure 33. Moiré fringe pattern on panel 9 at intermediate load level.

ORIGINAL PAGE IS
OF POOR QUALITY

ORIGINAL PAGE IS
OF POOR QUALITY

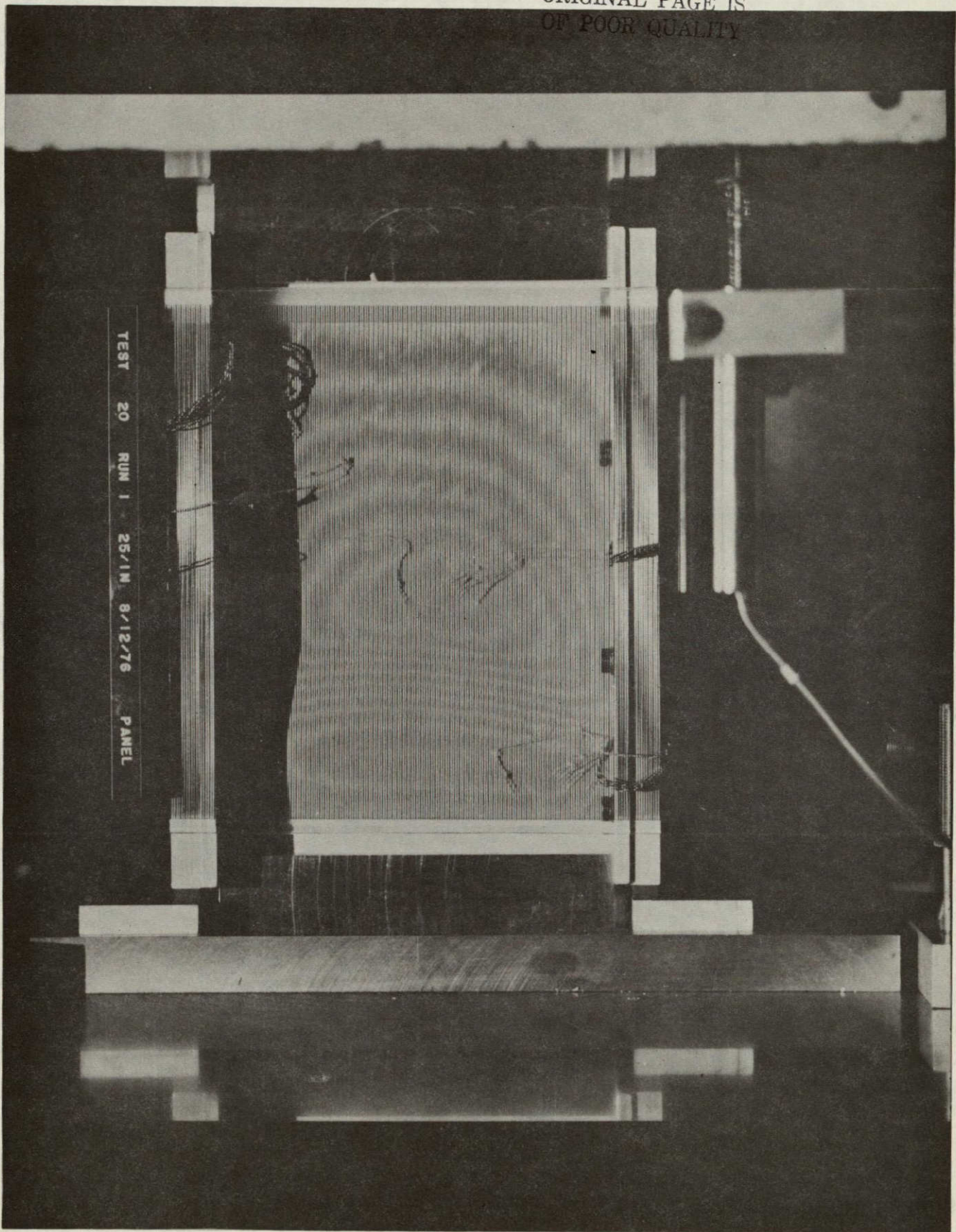


Figure 34. Moiré fringe pattern on panel 9 at panel failure.

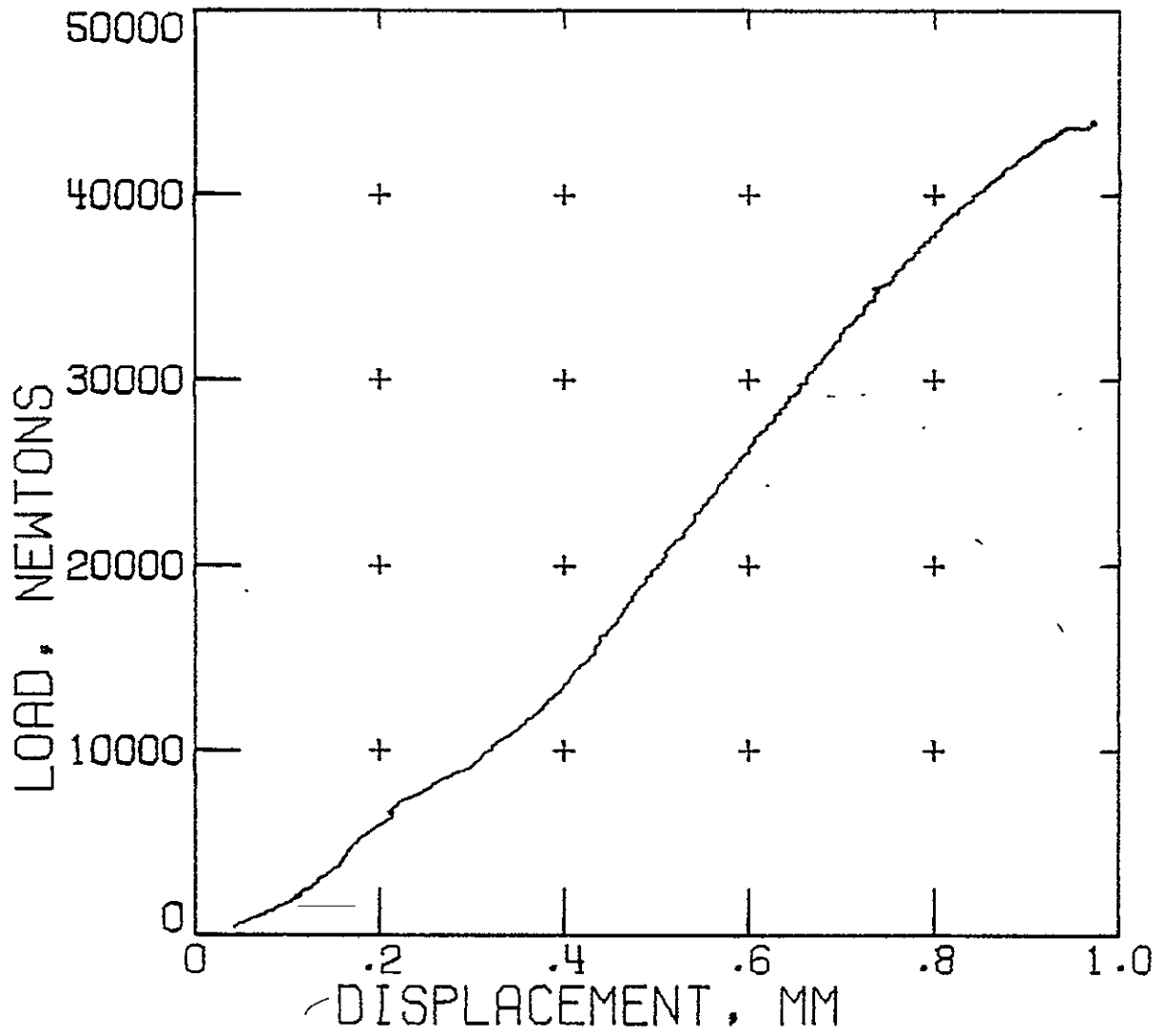


Figure 35. In-plane load-deflection behavior for panel 9.

REFERENCES

†

1. Kam, C.Y. and V.L. Freeman. An Exploratory Program to Evaluate Graphite-Polyimide Isogrid Structure. Final Report, MDC-G5893, Sep 1975.
2. Timoshenko, S. Theory of Elastic Stability. McGraw-Hill Book Company.